Jones, H. L., Westerhold, T., Birch, H., Hull, P., Hédi Negra, M., Röhl, U., Sepúlveda, J., Vellekoop, J., Whiteside, J. H., Alegret, L., Henehan, M., Robinson, L., van Dijk, J., Bralower, T. (2023): Stratigraphy of the Cretaceous/Paleogene (K/Pg) boundary at the Global Stratotype Section and Point (GSSP) in El Kef, Tunisia: New insights from the El Kef Coring Project. - Geological Society of America Bulletin, 135, 9-10, 2451-2477.

https://doi.org/10.1130/B36487.1

Heather Jones[ID]https://orcid.org/0000-0001-5795-5738
[†]hjones@marum.de.
GSA Bulletin; Month/Month 2022; v. 134; no. X/X; p. 000–000;
https://doi.org/10.1130/B36487.1; 12 figures; 3 tables; 1 supplemental file.
[1]Supplemental Material (6 figures, 2 tables, 2 data repository files). Please visit
https://doi.org/10.1130/GSAB.S.XXXX to access the supplemental material, and contact
editing@geosociety.org with any questions.
SCIENCE EDITOR: MIHAI DUCEA
ASSOCIATE EDITOR: CHRISTIAN KOEBERL
MANUSCRIPT RECEIVED 18 FEBRUARY 2022
REVISED MANUSCRIPT RECEIVED 10 SEPTEMBER 2022
MANUSCRIPT ACCEPTED MONTH 2022
Printed in the USA

Stratigraphy of the Cretaceous/Paleogene (K/Pg) boundary at the Global Stratotype Section and Point (GSSP) in El Kef, Tunisia: New insights from the El Kef Coring Project

Heather L. Jones[1,2,†], Thomas Westerhold[1], Heather Birch[3], Pincelli Hull[4], M. Hédi Negra[5], Ursula Röhl[1], Julio Sepúlveda[6], Johan Vellekoop[7,8], Jessica H. Whiteside[9], Laia Alegret[10], Michael Henehan[11], Libby Robinson[9], Joep van Dijk[6,7], and Timothy Bralower[2]
[1]MARUM–Center for Marine Environmental Sciences, University of Bremen, 28359 Bremen, Germany
[2]Department of Geosciences, Pennsylvania State University, University Park, Pennsylvania 16802, USA
[3]School of Earth Sciences, University of Bristol, Bristol BS8 1RJ, UK
[4]Department of Geology and Geophysics, Yale University, 210 Whitney Avenue, New Haven, Connecticut 06511, USA
[5]Faculty of Sciences of Tunis, University of Tunis El Manar, 2092 Tunis, Tunisia
[6]Department of Geological Sciences and Institute of Arctic and Alpine Research (INSTAAR), University of Colorado Boulder, UCB 450, Boulder, Colorado 80309-0450, USA
[7]Analytical, Environmental, and Geo-Chemistry, Vrije Universiteit Brussel, B-1050 Brussels, Belgium
[8]Department of Earth and Environmental Sciences, KU Leuven, 3000 Leuven, Belgium
[9]National Oceanography Centre Southampton, University of Southampton, Waterfront Campus, European Way, Southampton SO14 3ZH, UK
[10]Departamento de Ciencias de la Tierra & Instituto Universitario de Ciencias Ambientales, Universidad Zaragoza, 50009 Zaragoza, Spain
[11]GFZ German Research Centre for Geosciences, Telegrafenberg, 14473 Potsdam, Germany

ABSTRACT

The Cretaceous/Paleogene (K/Pg) boundary is marked by one of the largest mass extinctions in Earth's history, with geological evidence for this event being expressed in hundreds of locations worldwide. An extensively studied section located near El Kef, northwestern Tunisia, is characterized by the classic iridium-rich K/Pg boundary layer, abundant and well-preserved microfossils, and apparently continuous sedimentation throughout the early Danian with no previously described structural complication. These features led to its designation in 1991 as the Global Stratigraphic Section and Point (GSSP) for the base of the

Danian (i.e., the K/Pg boundary). However, the outcrop section has become weathered, and the "golden spike" marking the GSSP is difficult to locate. Therefore, the El Kef Coring Project aimed to provide a continuous record of unweathered sediments across the K/Pg transition in cores recovered from five rotary-drilled holes located close to the El Kef GSSP. Here, we present new, high-resolution lithologic, biostratigraphic, and geochemical data from these cores. The recovered stratigraphic successions of each hole (all drilled within ~75 m of one another) are unexpectedly different, and we identified a formerly unknown unconformity within planktic foraminiferal biozone P1b. Our results provide evidence that sedimentation at El Kef was not as continuous or free from structural complication as previously thought. Despite these challenges, we present a new composite section from the five El Kef holes and an age model correlated to the orbitally tuned record at Walvis Ridge, South Atlantic Ocean, which is critical in placing the paleoenvironmental and paleoecological records from El Kef in a global context.

INTRODUCTION

The mass extinction event at the Cretaceous/ Paleogene (K/Pg) boundary (ca. 66.02 Ma) eradicated more than 75% of marine species on Earth and is almost universally believed to have been caused by the asteroid impact that formed the Chicxulub crater off the modern- day Yucatán Peninsula in southern Mexico (e.g., Jablonski, 1991; Schulte et al., 2010; Hull et al., 2020). In addition to the demise of all non-avian dinosaurs, marine reptiles such as the mosasaurs, and many groups of invertebrates including the ammonites (e.g., Buffetaut, 1990; Sheehan and Fastovsky, 1992; Jablonski, 1994; Marshall and Ward, 1996), the K/Pg impact led to the extinction of over 90% of calcifying plankton (calcareous nannoplankton and planktic foraminifera), likely due to a combination of global cooling, decreased light availability, and possibly acidification of the surface ocean (e.g., D'Hondt et al., 1994; Bown, 2005; Ohno et al., 2014; Vellekoop et al., 2014, 2015, 2016; Kaiho et al., 2016; Henehan et al., 2019). These environmental perturbations led to substantial ecological reorganization throughout the marine food web as well as fundamental changes in oceanic carbon cycling that lasted for millions of years following the impact. This is particularly true in open-ocean depositional settings (e.g., D'Hondt et al., 1998; Coxall et al., 2006; Birch et al., 2016; Lowery et al., 2021), although neritic and bathyal regions closer to continental margins appear to have been more resilient (Sepúlveda et al., 2009, 2019; Rosenberg et al., 2021).

Geological evidence for the impact is recorded in hundreds of K/Pg sections studied worldwide but is expressed differently with distance from the Chicxulub crater (Claeys et al., 2002; Schulte et al., 2010; Lowery et al., 2018). In sections proximal to the crater, the K/ Pg boundary can be recognized by ejecta- and spherule-rich clastic event beds from 1 m thick to >80 m thick that were likely deposited by tsunamis and/or high-energy gravity flows (e.g., Bourgeois et al., 1988; Sigurdsson et al., 1991; Ocampo et al., 1996; Smit et al., 1992, 1996; Urrutia-Fucugauchi et al., 1996; Bralower et al., 1998; Alegret et al., 2005; Arenillas et al., 2006; Goto et al., 2008; Schulte et al., 2010, 2012; Gulick et al., 2019). The thicknesses of these complex clastic event beds generally decrease with increasing distance from the crater. In distal sections (>5000 km from the Chicxulub crater), the K/Pg boundary is typically expressed by a distinctive millimeter- to centimeter-thick clay layer (e.g., Molina et al., 2009) that is enriched in rare platinum-group elements (most notably iridium), shocked minerals, ejecta spherules, and Ni-rich spinels (e.g., Alvarez et al., 1980; Norris et al., 1999; Smit, 1999; Claeys et al., 2002; Schulte et al., 2010).

One of the most extensively studied distal sections is at the Global Stratotype Section and Point (GSSP) for the base of the Danian (i.e., the K/Pg boundary), located near the town of El Kef in northwest Tunisia (Molina et al., 2006; Fig. 1). Here, the K/Pg boundary "clay layer" is unusually thick in comparison to other stratigraphically complete marine sections (50 cm versus a few

centimeters), which has allowed for numerous high-resolution studies over the past decades (e.g., Perch-Nielsen et al., 1982; Smit and Romein, 1985; Brinkhuis and Zachari- asse, 1988; Keller and Lindinger, 1989; Arenil- las et al., 2000, 2004; Molina et al., 2006). The stratigraphically expanded sections at El Kef and other nearby outcrops (e.g., Elles and Aïn Settara; Fig. 1) contain well-preserved microfossils, which have provided a wealth of information about ecological, environmental, and climatological changes across the K/Pg boundary, including extinction and recovery patterns (e.g., Brinkhuis and Zachariasse, 1988; Speijer and Van der Zwaan, 1996; Arenillas et al., 2000, 2004; Rodríguez-Tovar et al., 2016; Alegret et al., 2022), carbon cycling and productivity (Sepúlveda et al., 2019), and global climate change (e.g., Galeotti et al., 2004; Vellekoop et al., 2015; MacLeod et al., 2018). However, the El Kef outcrop is heterogeneously weathered (Molina et al., 2009; Rodríguez-Tovar et al., 2016), and the "golden spike" placed to mark the exact position of the GSSP (Molina et al., 2006) is now either absent or very difficult to locate. The aim of the El Kef Coring Project was therefore to provide a continuous, expanded, and unweathered record across the K/Pg transition for future scientific analyses, especially using novel stratigraphic and geochemical techniques that require pristine material and were developed long after initial studies of the El Kef out- crop began.

Here, we present lithostratigraphic, biostratigraphic, bulk geochemical, and isotopic records from five sediment cores recovered between 2013 and 2015 during the El Kef Coring Project. These data provide the framework for an orbital age model that can be used to correlate the El Kef GSSP to other K/Pg boundary sections with unprecedented stratigraphic detail. The results of this study are therefore essential for placing future paleoceanographic, paleoecologic, and paleoclimatologic reconstructions from El Kef into a global context, and for providing the time control needed to determine the rates of biological and biogeochemical processes occurring in the aftermath of the Chicxulub impact.

BACKGROUND

Stratigraphy of the K/Pg Boundary at El Kef

The El Kef stratotype section is located ~5 km southwest of the town of El Kef in northwestern Tunisia (Figs. 1 and 2A). Here, Upper Maastrichtian to lower Paleogene strata are well- and continuously exposed, providing one of the most expanded and stratigraphically complete K/Pg boundary sections in the world (Keller and MacLeod, 1996; Molina et al., 2006). The boundary itself is included within the Upper Maastrichtian–Thanetian El Haria Formation, a 700-m-thick unit that is predominantly composed of gray marls and clays intercalated with thick, argillaceous limestone beds (Burollet, 1956; Zaghbib- Turki et al., 2001; Karoui-Yaakoub et al., 2002). The El Haria Formation lies conformably on the Campanian–lower Maastrichtian Abiod Formation, which is composed of fine- grained, chalky limestones with abundant macrofossils (inoceramids, bivalves, and echinoderms), ichnofossils, and microfossils (planktic foraminifera and calcareous nannofossils; Negra, 1994).

The K/Pg boundary at El Kef is defined by a "classic" 1–3-mm-thick, rust-colored ferruginous layer that comprises the iridium anomaly and contains hematite, goethite, pyrite, and <1 wt% $CaCO_3$ (Smit and Ten Kate, 1982; Keller and Lindinger, 1989; Robin and Rocchia, 1998; Molina et al., 2006). Below the K/ Pg boundary, the upper Maastrichtian sediments are represented by a 4.5 m series of white-gray marls with floating burrows (Keller, 1988a). Immediately overlying the K/Pg boundary is a 50-cm-thick, dark gray clay layer containing very few specimens of Cretaceous species (Smit, 1982; Keller, 1988a) and further impact materials, including Ni-rich spinels (Robin et al., 1991) and spherules of sanidine and hematite that are interpreted as altered microtektites (Smit, 1982; Robin et al., 1991). These dark gray clays grade into a lighter gray clay layer (50 cm thick), which progressively transitions into more carbonate-rich clays and eventually white-gray marls ~3 m above the K/Pg boundary, which are associated

with the diversification and increasing abundance of pelagic fauna and flora (Smit, 1982; Keller, 1988a; Pospichal, 1994).

Depositional Environment

During the Late Maastrichtian–early Paleogene, El Kef was located on the outer continental shelf/upper slope (~200–300 m water depth; e.g., Keller, 1988b; Speijer and Van der Zwaan, 1996; Alegret, 2003) of the Kasserine–Sidi Bouzid Island at a paleolatitude of ~25°N, on the southern margin of the "shallow" Tethys Sea that extended over much of northern Tunisia (Negra, 1994; Kadri et al., 2015; Negra et al., 2016; Negra and Jaballah, 2020; Fig. 1). The relatively high sedimentation rates (~1.1–3.5 cm/k.y.) within this outer shelf–upper bathyal environment during the latest Maastrichtian and early Danian (e.g., Cande and Kent, 1995; Adatte et al., 2002; MacLeod et al., 2018) indicate that the K/Pg transition and early Danian at El Kef is more stratigraphically expanded (>9 m in thickness) and complete than at pelagic sites, where it tends to be stratigraphically condensed (generally <1 m in thickness), and/or can contain short hiatuses or periods of non-deposition (Salaj, 1980; Zachos and Arthur, 1986; Pospichal, 1994; Adatte et al., 2002; Keller et al., 2002; Karoui-Yaakoub et al., 2002; Molina et al., 2009; Giron, 2013).

Although the sediments at El Kef were generally deposited in an oxic, open-marine environment, the dark color of the boundary clay layer and its relatively high pyrite and total organic carbon content (TOC; ~0.5%) may indicate a brief interval when conditions at the sediment/water interface became less oxygen-rich (Keller and Lindinger, 1989; Speijer and Van der Zwaan, 1996). Oxygen-deficient environments during the first 10–15 k.y. of the Danian at El Kef are supported by the ostracod faunas (Peypouquet et al., 1986) and depauperate benthic foraminiferal assemblages, which contain higher abundances of opportunistic taxa adapted to lower oxygen conditions (Alegret, 2003; Alegret, 2008). Furthermore, a 1–2‰ enrichment in δ15N above the K/Pg boundary may indicate enhanced bacterial denitrification (and thus lower oxygenation) and phytoplanktonic nitrate assimilation in response to elevated surface oceanic productivity (Sepúlveda et al., 2019). Intensively bioturbated sediments and the sequential re-appearance of many species of benthic foraminifera that had temporarily disappeared (due to the Lazarus effect) at the K/Pg boundary (Speijer and Van der Zwaan, 1996; Alegret et al., 2022) indicate well-oxygenated bottom waters following deposition of the boundary clay.

Tectonic and Eustatic History of Northwestern Tunisia

The stratigraphy in northwest Tunisia is structurally complex, with active tectonism affecting sediments deposited from the Late Cretaceous to the Neogene. Extensional tectonic activity with a WNW–ESE strike direction was first initiated in the Campanian–Maastrichtian and affected the entire North African margin (Bey et al., 2012; Fig. 2). These extensional processes led to the creation of a NW–SE to NNW–SSE conjugate normal fault system, which cross-cut and formed syn-depositional features within the carbonates of the Campanian Abiod Formation in the folded Atlasic domain (Bouaziz et al., 2002; Bey et al., 2012). Intervals of extensional tectonics were often followed by reverse or thrust faulting that led to structural inversion. In addition to active tectonism, northwestern Tunisia was also influenced by a complex eustatic history during the Late Cretaceous, with the Campanian experiencing sea-level transgression, followed by sea- level regression and relative cooling during the Late Maastrichtian (Stüben et al., 2002). Therefore, both tectonic and eustatic factors strongly controlled sediment deposition during the Late Maastrichtian in Tunisia.

Extensional tectonic plate movements were also active during the K/Pg boundary interval and gave rise to instabilities that widely affected continental platforms and ramps in the

Mediterranean Tethyan region (Bey et al., 2012; Negra et al., 2016). Evidence for this intense tectonic activity is observed in Tunisian outcrop sections as numerous faults and fractures with a dominant NW–SE to NNW– SSE trend (Fig. 2A), which is interpreted as representing reactivated Late Cretaceous faults. Normal fault motions initially gave rise to horst-graben structures followed by strike-slip movements that caused horizontal displacements of hundreds of meters. This faulting, along with relative sea-level changes, greatly impacted sedimentation during the Late Cretaceous and the Paleogene (Negra et al., 2016). Tectonic and eustatic processes have therefore caused structural complexity within the K/Pg boundary strata at El Kef that has generally been overlooked in previous studies, but which must be considered when investigating the stratigraphy of this section.

History of Studies at El Kef

As the K/Pg boundary section at El Kef provides one of the most stratigraphically complete and expanded records in the world, it has been the subject of numerous high-resolution studies over nearly half a century. Initially studied by Salaj (1974), the El Kef section was subsequently analyzed by a diverse suite of macro- and micro- paleontologists and geochemists, including for nannoplankton (Verbeek, 1977; Perch-Nielsen et al., 1982; Pospichal, 1994), planktic foraminifera (Keller, 1988a; Keller et al., 1996; Arenillas et al., 2000), benthic foraminifera (Keller, 1988b, 1992; Speijer and Van der Zwaan, 1996; Alegret, 2003, 2008; Alegret et al., 2022), dinoflagellates (Brinkhuis and Zachariasse, 1988; Brinkhuis et al., 1998; Vellekoop et al., 2015), palynoflora (Méon, 1990), ostracods (Donze et al., 1982; Peypouquet et al., 1986), ammonites (Goolaerts et al., 2004), ichnology (Rodríguez- Tovar et al., 2016), bulk rock chemistry (Keller and Lindinger, 1989), carbon, oxygen, nitrogen, and strontium isotopes (Keller and Lindinger, 1989; Vonhof and Smit, 1997; Sepúlveda et al., 2019), and platinum group elements (Smit and Ten Kate, 1982; Robin and Rocchia, 1998).

In 1989, the section was officially proposed as the GSSP for the base of the Danian (i.e., the K/Pg boundary) at the 28th International Geological Congress in Washington D.C., USA. In 1991, the International Commission on Stratigraphy ratified the proposal to define the GSSP at the base of the boundary clay at El Kef, after which the “golden spike” was placed at the section (Arenillas et al., 2000). Molina et al. (2006) published the official proposal, including the original definition and a proposition to define the K/Pg boundary as the moment of the asteroid impact, implying that all sediments generated by the impact belong to the Danian; a definition that is now generally accepted. Additional outcrops in close proximity to the El Kef GSSP provide other well-preserved, high-resolution K/ Pg boundary sections (Fig. 1), especially at Elles (75 km southeast of the El Kef outcrop), which has one of the most expanded orbitally calibrated K/Pg boundary records (Thibault et al., 2016) and has thus been proposed as a parastratotype of the K/Pg boundary (Zaghbib-Turki et al., 2001).

METHODS

Drilling Operations

The El Kef Coring Project initially planned to drill four holes, offset by ~25–50 m, near the El Kef GSSP outcrop section (36°09′13.2″N, 8°38′54.8″E; Molina et al., 2006; Fig. 2). A preliminary field survey conducted in 2011 was unable to locate the “golden spike” marking the exact position of the GSSP outcrop. However, a 0.5-m-deep trench located ~15 m NE of the GSSP (36°9′13.66″N, 8°38′55.16″E) uncovered fresh outcrop across the K/Pg boundary (MacLeod et al., 2018) and was used as a reference point for drilling operations (Fig. 2B). In December 2013, the first hole, Hole T, was rotary drilled to a depth of 60 m below surface (mbs) by the Laboratoire de sol Geoconseil, Tunisia. Hole T was designed to be an exploratory hole to determine the depth of the K/Pg boundary and therefore guide the drilling strategy for the

subsequent three holes. For this reason, the cores from Hole T were not drilled in core liners and were later cut into 1 m core sections. Between December 2013 and January 2014, the remaining three holes (holes A, B, and C) were each rotary drilled to a depth of ~36 m, and the cores were recovered in 1.5 m plastic core liners. The holes were drilled along a transect with Hole A (36°9′13.30″N, 8°38′56.02″E) located ~2 m to the south of Hole T, Hole B (36°9′12.66″N, 8°38′55.40″E) ~25 m to the southwest of Hole A, and Hole C (36°9′11.57″N, 8°38′54.44″E) ~40 m to the southwest of Hole B (Fig. 2B; Supplemental Material Fig. S11).

Following completion of drilling operations, the cores recovered from all four holes were sent to the International Ocean Discovery Program Bremen Core Repository at the MARUM–Center for Marine Environmental Sciences, University of Bremen, in Bremen, Germany, where core splitting and sampling was conducted in November 2014. The preliminary nannofossil biostratigraphy conducted during this initial sampling indicated that the K/Pg boundary was preserved in Hole A, but that holes B and C only contained the post-impact (Danian) sediments and not the boundary itself (see Results and Discussion). For this reason, it was decided that two additional holes, holes D and E, would be drilled in close proximity to Hole A to provide more sediment for scientific analyses immediately at and around the K/Pg boundary.

Hole D (36°9′13.30″N, 8°38′55.91″E) and Hole E (36°9′13.33″N, 8°38′56.01″E) were rotary drilled in March 2015 by the Laboratoire de sol Geoconseil, very close to Hole A (see Figs. 2B and S1). The drilling of both holes was destructive from 0 mbs to 4 mbs, with sediment cores being recovered in 1.5 m plastic core liners between 4 mbs and 26 mbs. All cores were sent to the core repository at the MARUM–Center for Marine Environmental Sciences, University of Bremen, where they were sampled in September 2017.

Split Core Analyses

Following their transportation to the MARUM core repository, all cores were kept refrigerated at +4 °C until the sampling party, when they were split into archive and working halves. To aid in core correlation, non-destructive X-ray fluorescence (XRF) scanning and digital line- scan imaging was conducted on the archive halves of each split core at the MARUM. The methodology for each of these technical analyses is outlined below.

Non-Destructive XRF

XRF core scanner data were collected every 1 cm down-core over a 1 cm^2 area directly at the split core surface of the archive half with a down- core slit size of 10 mm using generator settings of 10 kV, 30 kV, and 50 kV, a current of 1.0 mA, 1.0 mA, and 0.2 mA, and a sampling time of 15 s using an XRF Core Scanner II (Avaatech Serial No. 2). The split core surface was covered with a 4-µm-thin SPEX CertiPrep Ultralene 1foil to avoid contamination of the XRF measurement unit and desiccation of the sediment. The reported data were acquired by a Canberra X-PIPS Silicon Drift Detector (SDD; model SXD 15C-150-500) with 150 eV X-ray resolution, the Canberra Digital Spectrum Analyzer DSA-1000, and an Oxford Instruments 50W XTF5011 X-ray tube with rhodium (Rh) target material. Raw data spectra were processed by analyzing X-ray spectra with the iterative least squares software package (WIN AXIL) from Canberra Eurisys.

Line-Scan Imaging

In addition to the XRF data, digital line-scan images of the split cores were also obtained using the Avaatech XRF Core Scanner III, which has an option for line-scan camera and linear light source. The line scanner produces high-resolution color images and outputs accurate color data in RGB and Commission Internationale d'Eclairage (CIE) L (lightness), a (green to red chromaticity), and b (blue to yellow chromaticity) units (L*a*b*) using individual charge-coupled device (CCD) pixel calibration. The line-scan program uses the Stemmer Common

Vision Blox (CVB) platform to acquire and process color images. The camera system comprised a 3-CCD camera using 3 × 2048 pixels with a beam splitter and a manually controlled Pentax 50 mm lens. The image resolution is ~150 pixel/cm (70 μm/cm) in the cross-core and downcore directions. With an exposure time of 5 ms, a scan speed of 125 mm/s was achieved. Added to this time was the initialization time and camera repositioning after a scan. The image coverage was ~13.5 cm cross core and a maximum of 153 cm in the downcore direction. All split cores were measured using an aperture setting of 6.7 and 11 to account for the strong light-to-dark color changes in the cores.

Discrete Sample Analyses

Numerous geochemical and biostratigraphic analyses were performed on discrete samples from the El Kef cores to constrain the depth of the K/Pg boundary in holes A, D, and E, and to aid in stratigraphic correlation and the generation of an orbitally tuned age model. The methodologies employed for these analyses are outlined below.

Total Organic Carbon (TOC) and Weight Percent Calcium Carbonate (% $CaCO_3$)

Approximately 10 cm^3 of sediment was freeze-dried and ground to a fine powder using an agate mortar at the MARUM, University of Bremen. Total carbon (TC) and total organic carbon (TOC) were measured using a LECO CS-200 carbon-sulfur analyzer. Approximately 65 mg of the homogenized sample was weighed in a ceramic cup and burnt in an induction furnace. The evolved CO_2 was measured with a nondispersive infrared detector to provide a measure of the sedimentary TC content. To determine the TOC content, ~65 mg of powdered sample was decalcified using 12.5% HCl to remove carbonate species and analyzed as described above. Total inorganic carbon (TIC) was determined by subtracting TOC from TC. All data are reported in weight percent (wt%) dry sample, with an analytical precision of <3% based on replicate sample analysis.

Bulk Organic $\delta^{13}C$

Powdered sample was obtained by crushing freeze-dried sample using a benchtop IKA-Werke grinder. $CaCO_3$ was removed by reacting ~2 g of powdered sample with 40% HCl for 24 h, diluting with de-ionized water, and centrifuging until the samples attained a neutral pH. The carbon isotopic composition of the organic fraction ($\delta^{13}C_{org}$) was then measured using an isotope ratio mass spectrometer coupled with an elemental analyzer (EA-IRMS) at the School of Ocean and Earth Science, University of Southampton, UK, with USGS-40 and USGS-41a as the international reference standards used to calibrate the data with an analytical precision of 0.01‰.

Bulk Carbonate $\delta^{13}C$ and $\delta^{18}O$

For El Kef A and a subset of samples from El Kef E (see Supplemental Data 1, Table A5), the bulk carbonate was sonicated in MeOH and dried for 24 h at 50 °C. The samples were then reacted with 106.2% phosphoric acid in a Thermo Finnigan Kiel-IV carbonate device at the National Oceanography Centre, University of Southampton. Purified CO_2 was analyzed on a Thermo Finnigan MAT 253 isotope ratio mass spectrometer. Carbon and oxygen stable isotope ratios were normalized using a two-point calibration with GS1 (in-house material was previously calibrated to NBS 18 and NBS 19) and NBS 18 (International Atomic Energy Agency, Vienna, Austria). An in-house reference material (SC1) was used as an independent quality control with an overall precision of 0.01‰ and 0.04‰ for $\delta^{13}C$ and $\delta^{18}O$, respectively.

For El Kef C, D, and a subset of samples from El Kef E (see Supplemental Data 1, Table A5), additional bulk carbonate C and O isotope measurements were made at the Yale Analytical and Stable Isotope Centre (YASIC), Yale University, also on a Thermo-Finnigan MAT 253 mass spectrometer coupled to a Thermo Finnigan Kiel IV carbonate device. Analytical precision of replicates of standard measurements was typically better than 0.06‰ and 0.08‰ for carbon and

oxygen, respectively. To verify consistency between laboratories, the University of Southampton in-house reference materials (GS1 and SC1) were measured at YASIC, with both labs agreeing within accepted standard error (instrument and material) of 0.1‰ ($\delta^{18}O$) for both reference materials.

Nannofossil Biostratigraphy

Nannofossil biostratigraphy was performed on at least one sample per core in holes B, C, and D and at least five samples per core in holes A and E with the frequency increasing close to the boundary in Hole A. Smear slides were prepared for biostratigraphy by disaggregating a small chip of sediment in distilled water. An aliquot of this mixture was applied to a cover slip, dried on a hot plate, and adhered to a microscope slide using Norland Optical Adhesive, which was then cured under ultraviolet light. All smear slides were examined at 1600× magnification under cross-polarized light using a ZEISS Axio Imager.A2m (at Penn State University, State College, Pennsylvania, USA) or an Olympus BX51 polarization microscope (MARUM, University of Bremen). Age-diagnostic nannofossil specimens were imaged using a ZEISS Axiocam 305 color camera (Penn State University) or an Olympus DP22 camera and associated software (MARUM, University of Bremen) to help identify specimens to species level and to allow for internal taxonomic consistency. The nannofossil biostratigraphy utilized largely follows the Paleogene coccolith (CP) zonation of Okada and Bukry (1980) and the additional Paleocene calcareous nannofossils (CNP) biozones proposed by Agnini et al. (2014).

Planktic Foraminiferal Biostratigraphy

For the uppermost Maastrichtian and lower Danian, planktic foraminiferal biostratigraphy was conducted on 58 samples from Hole A, 34 samples from Hole C, and 52 samples from Hole E. Holes B and D were not sampled for planktic foraminifera. All samples were oven-dried at 40°C, weighed to obtain bulk dry sample weight, and soaked and disaggregated in a cold sodium hexametaphosphate (Na6(PO3)6) solution, then washed with tap water or deionised water over 38 μm or 63 μm wire mesh sieves, in accordance with each laboratory's standard protocols. The residue was oven-dried at 40 °C and weighed. Presence/absence data were recorded for each split sample by picking ~300 specimens, which were identified to the species level using the taxonomic concepts in the Paleocene Atlas of Olsson et al. (1999). The remainder of the sample was then quickly scanned to check for rare species. Planktic foraminiferal biostratigraphy followed the Pardo et al. (1996) biozonation scheme for the Cretaceous and the Wade et al. (2011) biozonation scheme for the Paleocene.

Below the K/Pg boundary, 25 additional samples were examined from Hole A (cores 21–26, 26.88–36.32 mbs) to determine the first occurrence (FO) of *Plummerita hantkeninoides,* which marks the base of the uppermost Maastrichtian planktic foraminiferal biozone (Pardo et al., 1996). Samples were sieved to >106 μm, and multiple splits of ~500 particles were examined to determine the presence or absence of *Plummerita hantkeninoides* following the taxonomic concepts of Brönnimann (1952). After initial screening, more detailed treatment (up to 19 splits) was given to samples around the provisional FO.

Paleomagnetism

Paleomagnetic analyses were conducted at the University of Bremen on 54 samples from Hole A (18), Hole B (19), and Hole C (17), collectively spanning the entire recovered stratigraphic range. Each sample was demagnetized for natural remanent magnetization (NRM) in 2.5 mT increments to 10 mT AF, at which the sensitivity of the magnetometer was reached. Unfortunately, magnetic intensities were weak throughout the section such that consistent and reliable polarity could not be reconstructed from the inclination and declination data. For this reason, it was not possible to generate a paleomagnetic record for the El Kef cores.

RESULTS

Following data collection, our first aim was to constrain the position of the K/Pg boundary in holes A, D, and E to provide a basic stratigraphic frame of reference. The boundary was initially identified by observed lithological changes on the split core surfaces and by preliminary nannofossil biostratigraphy, specifically the abrupt decline in Cretaceous species and the replacement by an assemblage dominated by disaster species. The K/Pg boundary depth interval was subsequently confirmed with geochemistry, namely the sharp decline in $\%CaCO_3$ and the abrupt decrease in bulk carbonate $\delta^{13}C$ (Fig. 3). This combination of nannofossil biostratigraphy and geochemistry shows nearly identical changes in the outcrop section (e.g., Keller and Lindinger, 1989; Pospichal, 1994), where shifts also correspond to traditional boundary markers including iridium and Ni-rich spinels (Kruslys and Krahenbuhl, 1983; Robin et al., 1991; Robin and Rocchia, 1998), which validates the boundary definition in the cores. Once the position of the K/Pg boundary was constrained, we then conducted more detailed lithostratigraphic, biostratigraphic, and geochemical analyses on the rest of the Maastrichtian and Danian sediments, the results of which are outlined below.

Lithostratigraphy

The El Kef cores consist predominantly of gray marls (carbonate-rich mudstones) that have been moderately to intensively bioturbated (Fig. 4G), except for immediately above the K/Pg boundary. Structural complexity at this site is evidenced by abundant microfractures and, less commonly, larger fractures filled with sparry calcite cement or pyrite (Figs. 4C–4E). At least one unconformity is also present during the lower Paleocene (Fig. 4B). In addition to the inherent structural complexity of these cores, rotary drilling disturbance including common biscuiting (artificial layering created when the formation is fractured during coring and drilling mud is injected between layers) and flow-in after coring (Fig. 4I) affected the sediments to a varying extent. Moreover, the top three to four cores(~4.5–6 m) from each hole are strongly weathered (Fig. 4F), obscuring many of the features that would otherwise be visible on the split-core surfaces. Although these confounding factors complicate the stratigraphic reconstruction of this section, many critical sedimentological features are nevertheless observed and described in the El Kef cores. Below, we separate our detailed lithostratigraphic findings into two sections: holes A, D, and E, and holes B and C, which— based on the biostratigraphic results—represent the earlier and later parts of the recovered stratigraphic interval, respectively.

Holes A, D, and E

At El Kef, the K/Pg boundary can be recognized by a transition from lighter gray, carbonate-rich Cretaceous sediments to darker gray Paleocene marls in Hole A (Core 16R-1, ~108 cm, 20.03 mbs), Hole D (Core 10R-1, ~73 cm, 18.31 mbs), and Hole E (Core 10R-1, ~121 cm, 19.15 mbs) (Figs. 3 and 4A). The distinctive 1–3 mm, rust-colored layer enriched in rare earth elements that is characteristic of the K/ Pg boundary in the El Kef outcrop is noticeably absent from the El Kef cores. This is most likely a product of the rotary drilling process, which either completely removed this very thin layer or “smeared” it into the over- and/or underlying sediments.

The Upper Maastrichtian sediments below the K/Pg boundary at El Kef generally consist of dark gray marls containing visible foraminifera. Darker-colored sediment layers were observed between El Kef A 20R-1A, 0 cm, and El Kef A 21R-1A, 65 cm (~25.28–27.53 mbs), and from El Kef A 22R-1A, 100 cm, to El Kef A 25R-1A, 150 cm (~29.32–34.72 mbs; Fig. 3). Large burrows and other evidence for moderate to intense bioturbation were observed throughout the uppermost Cretaceous, including immediately below the K/Pg boundary (Fig.

4A). Fracturing is relatively uncommon throughout the Maastrichtian at El Kef, especially when compared to the Paleocene cores (see below).

Immediately above the K/Pg boundary, the marls are much darker in color than in the uppermost Cretaceous, and there is little evidence for bioturbation (Fig. 4A). Intervals containing abundant pyrite are also common (e.g., El Kef A 15R-1A, 0–69 cm, 17.68–18.37 mbs). Above the base of Core 14 in Hole A (17.6 mbs) and the base of Core 9 in holes D and E (17.48 mbs and 17.84 mbs, respectively), the sediments become lighter in color and there is a slight increase in bioturbation. However, bioturbation remains low until ~14R-1A, 76 cm in Hole A (17.51 mbs), 8R-1A, 135 cm in Hole D (15.67 mbs), and 8R-1A, 148 cm in Hole E (16.22 mbs), above which there is a visible increase in bioturbation that includes the reappearance of small, bedding-parallel burrows (Fig. 4G). The exact depth level at which this increase in bioturbation occurs is difficult to determine due to the presence of common rotary drilling marks and other effects of drilling disturbance such as heavy biscuiting and flow-in (especially in Hole A; Fig. 4I), and abundant microfractures that obscure other primary and secondary structural features on the split-core surfaces (Figs 4C– 4E). These microfractures are rare in the Upper Maastrichtian sediments but are common throughout the lowermost Danian (especially in Hole E), which suggests that they were not caused by drilling disturbance. Typically, the fractures are thin, infilled with a white mineral (likely sparry calcite), and are bedding-parallel or low-angle oblique (Fig. 4D). It is also common for fractures to abruptly switch from being bedding parallel to low-angle oblique (and vice versa) (e.g., El Kef E 9R-1A, 122–128 cm, 17.56–17.62 mbs), or for the low-angle fractures to change strike direction (e.g., El Kef E 8R-1A, 88–89 cm, 15.62–15.63 mbs). Although intermittent fracturing was observed throughout the entirety of the lower Danian at El Kef, extended intervals of heavy fracturing generally occur closer to the K/Pg boundary (e.g., El Kef E 8R-1A, 58–148 cm (15.32–16.22 mbs), and El Kef E 9R-1A, 122–140 cm (17.56–17.74 mbs). In addition to these thin microfractures, some larger, high-angle fractures that cross-cut bedding direction were observed (e.g., El Kef E 9R-1A, 84–97 cm, 17.18–17.31 mbs), one of which contained partially oxidized material and/ or pyrite (El Kef E 6R-1A, 49–67 cm, 11.96– 12.14 mbs; Fig. 4D).

At a depth of ~14.8 mbs in Hole D (8R-1A, 48 cm) and ~10.08 mbs in Hole E (5R-1A, 21 cm), there is a sharp transition from lightly bioturbated, dark gray-colored marls to more heavily bioturbated, lighter-colored sediments (Fig. 4B). It is likely that this lithologic boundary represents an unconformity, which is supported by both the nannofossil and planktic foraminiferal biostratigraphic datums (see Biostratigraphy section). The unconformity is observed at a lower depth in Hole D (~14.8 mbs) than in Hole E (~10.08 mbs), which suggests that an offset exists between the two holes that was potentially caused by a reactivated minor fault (Fig. 2B; see Discussion for further detail). Unfortunately, the contact between the older, darker-colored marls and the younger, lighter-colored sediments is partially obscured by drilling disturbance in both holes D and E, so its exact nature cannot be described in detail. Similar drilling disturbance is also observed at the top of Core 14 in Hole A (14R-1A, 0–29 cm, 16.75–17.04 mbs; Fig. 4I), which suggests that the unconformity is present in this hole but has been completely obscured by cave-in.

Above the unconformity in Hole E, the drilling disturbed, lighter-colored sediments continue until El Kef E 4R-1A, ~81 cm (9.05 mbs), above which the cores start to become heavily weathered and/or oxidized (Fig. 4F). In Hole D, the sediments above the unconformity are heavily fractured and intensely bioturbated, with intervals that contain concentrated small, bedding-parallel burrows (e.g., El Kef D 7R-1A, 110–114 cm, 13.79–13.82 mbs) and others that contain larger, elongated burrows that cross- cut bedding planes (El Kef D 7R-1A, 15 cm, 12.84

mbs). Most of the fractures (especially throughout El Kef D, 6R-1A, 11.05–12.59 mbs) are longer and wider than those observed lower in the Danian and generally cross-cut bedding planes in a NW–SE direction. Above El Kef D, 5R-1A, ~44 cm (9.86 mbs), the sediments are still heavily bioturbated but there is reduced fracturing. Weathering and oxidation begin to affect the sediments in Hole D from the base of 3R-1A (7.89 mbs), although it only obscures sedimentary features on the split-core surfaces in cores 1 and 2.

Overall, the sharp facies transitions and intense fracturing/micro-fracturing observed in the cores confirm the effect of tectonics on sedimentation during the earliest Danian. The larger microfractures appear to be associated with the movement of the regional NW–SE- trending faults (Fig. 2A). These structures are also possibly responsible for the offset in the depth of the identified unconformity between holes D and E.

Holes B and C

Higher in the Danian, the lighter gray-colored marls observed above the unconformity in holes D and E continue. These sediments are generally more intensely bioturbated and less heavily fractured than lower in the Danian, although there are sporadic, restricted intervals where more severe microfracturing occurs (e.g., El Kef B 23R-1A, 118–149 cm, 35.28–35.59 mbs, and El Kef C 21R-1A, 53–67 cm, 31.33–31.47 mbs; Figs. 4C and 4D). Extended intervals of intense microfracturing are rarer than in holes D and E but can also be observed in El Kef B 13R- 1A, 105 cm, to 15R-1A, 123 cm (19.16–22.53 mbs), and El Kef C 8R-1A, 99 cm, to 9R-1A, 146 cm (11.09–13.16 mbs). These concentrated microfractures are usually low-angled and SW– NE-trending but often become more parallel. In addition to microfractures, larger NW–SE- or SW–NE-trending fractures filled with sparry calcite cement were observed. These fractures are not as common as the microfractures (which they cross-cut) and are confined to restricted stratigraphic intervals (e.g., El Kef B 11R-1A, 0–25 cm, 14.9–15.15 mbs and 52–75 cm, 15.42–15.65 mbs, and El Kef C 19R-1A, 76–93 cm, 28.36–28.53 mbs).

Pyrite nodules are sporadically observed throughout holes B and C, particularly in the deeper cores. Two of these pyrite nodules (El Kef B 18R-1A, 116–117 cm, 27.26–27.27 mbs and 119–120 cm, 27.29–27.30 mbs) were observed immediately below a SW–NE-trending contact that may represent a microfault (EL Kef B 18R- 1A, 115–120 cm, 27.25–27.5 mbs; Fig. 4D). Pyrite was also observed lining the edges of burrows (El Kef B 18R-1A, 49 cm, 26.59 mbs; Fig. 4G) and completely replacing them (e.g., El Kef C 23R-1A, 46 cm, 34.46 mbs). Burrows themselves are a common feature throughout El Kef B and C and are generally larger (El Kef C 23R-1A, 21–23 cm, 34.21–34.23 mbs) and more complex (El Kef B 17R-1A, 115–117 cm, 25.65–25.67 mbs and El Kef B 13R-1A, 55–60 cm, 18.65–18.7 mbs) than those observed in the lower Danian sediments of holes A, D, and E (Fig. 4G). Ichnofossils become more diverse and increase in abundance up-section, especially long, cylindrical, bedding-parallel forms (e.g., El Kef B 8R-1A, 12–23 cm, 10.22–10.33 mbs; Fig. 4G).

Within El Kef B 11R-1A and El Kef C 14R- 1A, parallel laminations of alternating darker and lighter sediments develop (Fig. 4H) and become low-angled within El Kef B 5R-1A and El Kef C 13R-1A, 76–79 cm (18.86–18.89 mbs; Fig. 4H). These laminae are continuously present near the top of Hole B but temporarily disappear in Hole C between El Kef C 7R-1A, 41 cm, and the base of El Kef C 10R-1A, 8.91–14.8 mbs. Cores 1 through 4 in holes B and C are intensely weathered, so meaningful lithological observations cannot be made.

Biostratigraphy

High-resolution calcareous nannofossil biostratigraphy was predominantly conducted on samples from Hole E, which was discovered to contain the thickest succession of lowermost Danian sediments (Fig. 3). Lower-resolution nannofossil biostratigraphy (at least one sample per

core) was performed on sediments from all other holes. In contrast, planktic foraminiferal biostratigraphy was only conducted in holes A, C, and E and not in holes B or D. Both the calcareous nannofossil and planktic foraminiferal biostratigraphy for all of the El Kef holes was complicated by clear evidence for local faulting and fracturing (Figs. 4C–4E), which causes some biozone markers to disappear and then reappear again further up section. The effects of primary faulting on the biostratigraphy are further complicated by frequent drilling disturbance and drill mud contamination (Fig. 4I; see Lithostratigraphy for further information).

Calcareous Nannofossil Biostratigraphy

The uppermost Maastrichtian observed in El Kef holes A, D, and E is characterized by well- preserved nannofossils with moderate amounts of etching and overgrowth (Fig. 5). Assemblages are highly diverse and comprised of typical latest Cretaceous taxa including *Watznaueria barnesiae*, *Prediscosphaera cretacea*, *Prediscosphaera stoveri*, *Micula murus*, *Micula prinsii*, *Lithrapidites quadratus*, *Cribrosphaerella ehrenbergii*, *Eiffellithus turriseiffelii*, and *Arkhangelskiella cymbiformis*, all of which are commonly reworked into the overlying earliest Danian sediments. *Micula prinsii* extends to the base of Hole A, which indicates that this section lies within the uppermost Maastrichtian and is within 0.25 m.y. of the K/Pg boundary (Henriksson, 1993).

The K/Pg boundary can be recognized in nannofossil smear slides by the extinction of nearly all Cretaceous species and the increased abundance of calcareous dinoflagellate cysts (Fig. 5: 19 and 25). Using these criteria, the K/Pg boundary was found to be expressed in three of the five holes drilled at El Kef (holes A, D, and E; Table 1). Nannofossil preservation above the K/Pg boundary is generally moderate to good with abundant complete cell coverings (coccospheres) throughout (Fig. 5: 15), and abundant fragile specimens of *Neobiscutum* in the lower- most Danian (Fig. 5: 13–14). Within each hole, we identified the FOs of *Cruciplacolithus primus* (base of the *Cr. primus* subzone; Bernaola and Monechi, 2007), *Coccolithus pelagicus* (Base CNP2; Agnini et al., 2014), and *Cruciplacolithus intermedius* (Bernaola and Monechi, 2007; Table 1), all of which are illustrated in Figure 5. Despite intensive and detailed biostratigraphic work, the exact placement of these datums was complicated by several factors. Firstly, many of the earliest "primitive" specimens of incoming Paleocene taxa (e.g., *Cr. primus*) look very different from their fully evolved counterparts both in size and form (see Fig. 5: 5–9), and this poses a particular challenge for correlation to more stratigraphically condensed deep-sea sections, where such primitive forms have not been described. Moreover, as the cores are strati-graphically expanded, nannofossil specimens that are transitional in form between two species are common. For example, it is often difficult to differentiate *Cr. primus* from *Cr. intermedius* at El Kef, as these two species are generally separated by size (smaller or larger than 7 μm for *Cr. primus* and *Cr. intermedius*, respectively), which is particularly problematic when there is any evidence of calcite overgrowth. Other than size, some nannofossil paleontologists use additional, and somewhat variable, criteria to differentiate between *Cruciplacolithus* species, and there has been considerable discussion as to which of these described forms and taxonomic classifications are best used as datums or biozone markers (e.g., Bernaola and Monechi, 2007; Agnini et al., 2014; Thibault et al., 2018). Applying the traditional 7 μm "cut-off" between *Cr. primus* and *Cr. intermedius* in our study, the FO of *Cr. intermedius* occurs immediately above the unconformity that is present in holes A and D, and ~1 m below the unconformity in Hole E (see Lithostratigraphy; Figs. 3 and 4B). Similarly, it was not possible to reliably identify the base of CNP3 (Agnini et al., 2014), which is defined by the FO of the *Prinsius dimorphosus* group (including *Praeprinsius tenuiculus*). Very small (~1–2 μm) *Praeprinsius* specimens (*Praeprinsius* cf. *vegrandis*; Kim, 2020) originate shortly above the K/Pg boundary at El Kef (El

Kef E 10R-1W, 81 cm), and appear to gradually evolve into *Pr. tenuiculus* throughout the early Danian (Fig. 5: 16–18). Therefore, it is challenging to determine the FO of "true" *Praeprinsius tenuiculus* in the El Kef cores without extensive morphometric work beyond the scope of this contribution.

Holes B and C, which do not preserve the K/Pg boundary and represent a later part of the Danian post-extinction interval, did not contain any of the usual age-diagnostic nannofossil taxa such as *Chiasmolithus danicus* (Base CP2; Okada and Bukry, 1980), *Prinisus martinii* (Base CNP4; Agnini et al., 2014), and *Toweius pertusus* (Base CNP5; Agnini et al., 2014), or contain the last occurrence (LO) of the *Prinsius dimorphosus* group (Agnini et al., 2014). Extremely rare primitive specimens of *Cruciplacolithus tenuis* (Base NP2; Martini, 1971) that lack the fully-developed "feet" diagnostic of this species are observed in only two samples (El Kef C 7R-1W, 61 cm and El Kef C 3R-1W, 1 cm; Fig. 5: 1 and 2); however, a true FO or stratigraphic range can- not be determined. Therefore, it was not possible to constrain the biostratigraphic ages of holes B and C using nannofossil datums.

Planktic Foraminiferal Biostratigraphy

High-resolution planktic foraminiferal biostratigraphy was conducted on the Maastrichtian sediments from Hole A and on the early Danian sediments (including the K/Pg boundary when present) from Hole A (up until the cave-in at the top of Core 14, ~17.05 mbs), Hole C, and Hole E (Fig. S2). Planktic foraminiferal biostratigraphy was not conducted on holes B and D. In the uppermost Maastrichtian, planktic foraminifera are moderately preserved, although with pervasive infilling from secondary carbonate. Assemblages are diverse, consisting of typical Maastrichtian *Globotruncana*, *Globotruncanella*, *Globotruncanita*, *Hedbergella*, *Heterohelix*, *Pseudoguembelina*, *Racemiguembelina*, *Pseudotextularia*, and *Rugoglobigerina* species. The species *Plummerita hantkeninoides* is present throughout the Maastrichtian cores examined, down through sample El Kef A 25R-1W, 75–77 cm (33.88 mbs), in which two individuals were observed. *P. hantkeninoides* is absent in the next deepest sample examined (El Kef A 25R-1W, 103– 107 cm, 34.17 mbs) and in all of the samples below this depth interval. Although a transitional form was observed in sample El Kef A 25R-1W, 127–130 cm (34.405 mbs), this single specimen more closely resembles *Rugoglobigerina reicheli* and was therefore not considered to be a true *P. hantkeninoides*. For this reason, the base of the *P. hantkeninoides* biozone is placed at the midpoint between sample El Kef A 25R-1W, 75–77 cm, and El Kef A 25R-1W, 103–107 cm (34.025 mbs; Table 1).

The K/Pg boundary (i.e., base of planktic foraminiferal zone P0) can be recognized by the extinction of almost all Cretaceous taxa (e.g., *Globotruncana*, *Rugoglobigerina*, and *Globigerinelloides*; Wade et al., 2011). The placement of the K/Pg boundary using planktic foraminiferal biostratigraphy is consistent with the nannofossil biostratigraphy in Hole A but shows a +~35 cm offset in Hole E (Table 1). Above the K/Pg boundary, planktic foraminifera are poorly preserved and assemblages are less diverse than at open ocean sites. The FO of *P. eugubina* (base Pα) occurs at a depth of 19.39 mbs in Hole A and 18.72 mbs in Hole E (Fig. 3; Table 1). However, these earliest specimens are non-typical (containing only 4.5 to 5 chambers), with classic 6–7-chambered forms not appearing until sample El Kef A 16R-1W, 8–9 cm (~19.07 mbs) and not being observed at all in El Kef E, although this may be because only the 38–63 μm size fraction was examined in most samples from this hole. This depth level is coincident with an increase in the abundance of biserial planktic foraminifera, which occurs at ~19 mbs and ~16.05 mbs in holes A and E, respectively. At the very top of their stratigraphic range (between El Kef E 7R-1W, 65–67 cm, 13.77 mbs and El Kef E 7R-1W, 125–127 cm, 14.37 mbs), *P. eugubina* specimens are very rare. Despite this, we were still able to reliably

identify the LO of this taxon (base biozone P1a) within both holes A and E (Table 1). Overall, the stratigraphic range of *P. eugubina* (i.e., the "thickness" of Pα) spans ~2 m of sediment in Hole A and >4.5 m of sediment in Hole E (Figs. 3 and S2), which confirms that Hole E contains a thicker succession of earliest Danian sediments than Hole A despite the fact that the two holes were drilled within ~5 m of each other.

The FO of *Subbotina triloculinoides* (base biozone P1b) was recognized immediately above the unconformity in Hole E (~12.38 mbs) but was not observed in Hole A (Table 1) as planktic foraminiferal biostratigraphy was not conducted above ~17.13 mbs in this hole. At the base of Hole C, which lies farther above the unconformity, planktic foraminiferal assemblages contain *Globanomalina compressa*, which places these sediments firmly within biozone P1c. As the P1b/P1c boundary was not observed in any of the three holes examined (holes A, C, and E), it is possible that this time slice (spanning <1.2 m.y.) was not preserved in any of the cores recovered or that it is contained within the weathered cores at the top of Hole E (cores 2–4), which were not sampled for planktic foraminiferal biostratigraphy due to poor preservation. Alternatively, this stratigraphic boundary may be preserved at El Kef but not expressed in our recovered cores due to the same local or regional tectonic processes (e.g., faulting) that led to each of our drilled holes containing slightly different parts of the Upper Maastrichtian and/or lower Danian. The presence of a second unconformity above the one located at El Kef E 5R-1W, 21 cm (~10 mbs), is also possible, and we explore this in further detail in the Discussion.

The base of biozone P2 was tentatively placed between samples El Kef C 14R-1W, 73–76 cm (~20.45 mbs) and El Kef C 14R-1W, 123–126 cm (20.95 mbs; midpoint ~20.7 mbs; Table 1), at the FO of *Praemurica uncinata*. Very rare *P. uncinata* specimens were also observed in sample El Kef C 20R-1W, 93–96 cm (30.15 mbs). However, this taxon was noticeably absent from the next nine samples examined above this depth level (i.e., between samples El Kef C 14R-1W, 123– 126 cm, and El Kef C 20R-1W, 38–41 cm, 20.95–28.65 mbs), which suggests that its isolated presence at a sample depth of 30.15 mbs is a product of downhole drilling contamination. Furthermore, if the P1c/P2 biozone boundary were to be placed as far down as ~30.15 mbs in Hole C, the FOs of near-contemporary nannofossil taxa such as *Chiasmolithus danicus*, *Cruciplacolithus tenuis*, *Prinsius martinii*, and *Toweius pertusus* would be observed at similar or lower depths (e.g., within El Kef C 20R-1W or below). In addition, *Praeprinsius tenuiculus* should be absent from almost all Hole C samples. However, *P. tenuiculus* is present in high abundances throughout the entirety of Hole C, and the FOs stated above were not observed in any of the nannofossil samples from this hole. We therefore consider the consistent presence of *P. uncinata* starting at ~20.7 mbs as its true FO.

Geochemistry

Total Organic Carbon (TOC)

The oldest part of the Maastrichtian that was recovered at El Kef (between ~29.40 and 36.04 mbs, Hole A) is characterized by relatively stable TOC contents (~0.75 wt%; Fig. 3D). Above this interval in Hole A and above the bottom-most sample analyzed in Hole E (~27.73 mbs), TOC values gradually decrease to ~0.5 wt% up until the K/Pg boundary. Above the extinction horizon (~20 mbs, Hole A and ~19.4 mbs, Hole E), TOC content begins to increase up to a maximum of 1.13 wt% at 17.26 mbs (Hole A) and up to a maximum of 1.3 wt% at 17.05 mbs (Hole E). TOC values in Hole E then remain at ~1% until ~13.77 mbs, where there is a sharp, transient increase to TOC values exceeding 1.5 wt%. Between 13.37 mbs and 12.08 mbs in Hole E, TOC decreases back down to ~0.7 wt% and remains at a relatively stable value until the unconformity at ~10.08 mbs, above which TOC content decreases further (<0.5 wt%). In Hole A, the decrease to similarly low TOC values occurs further down than in Hole E (~17.15

mbs). This is consistent with our previous suggestion that cave-in obscures the unconformity within Hole A, Core 14 (see Lithostratigraphy). Further above the unconformity (i.e., in holes B and C, and the upper part of Hole A), TOC content remains low, generally ranging between 0.3 and 0.7 wt% (Fig. 6C). The decrease to very low values (~0.1 wt%) at the top of each hole is most likely a product of weathering.

Calcium Carbonate Content

In the Maastrichtian, the weight percent calcium carbonate content ranges between ~10 and 50% and averages ~37.5% (Fig. 3E). At ~20.025 mbs in Hole A and 19.175 mbs in Hole E, $CaCO_3$ content sharply decreases to <10 wt%, representing the "carbonate crash," which is characteristic of the K/Pg mass extinction. However, although the depth level of the $CaCO_3$ decrease is consistent with the LO of Cretaceous calcareous nannoplankton taxa in both holes A and E, the LO of Cretaceous planktic foraminifera is observed 20 cm higher than the carbonate crash in Hole A and ~30 cm lower than it in Hole E. The depth discrepancy between the extinction of planktic foraminifera and the decrease in $CaCO_3$ values in Hole E can likely be explained by the fact that only planktic foraminiferal samples from the 38–63 µm size fraction were examined from this hole. Therefore, some of the larger Cretaceous species may only have been present in sediments from the > 63 µm size fraction and thus were not observed in our study. In contrast, the depth discrepancy in Hole A may be due to the short-term persistence of some smaller planktic foraminiferal species into biozone P0, as previously recognized in other stratigraphically expanded K/Pg sections (e.g., Strong, 2000; Arenillas et al., 2004; Keller, 2004; Rasmussen et al., 2005).

Above the K/Pg boundary in El Kef A (~20.025 mbs), $CaCO_3$ content remains relatively low (average of 13–14 wt%) up to ~18.25 mbs. Between 18.25 mbs and ~17 mbs, $CaCO_3$ values then increase gradually to just over 40 wt% (Fig. 3E). Higher up-section, a further increase to even higher $CaCO_3$ contents (~60 wt%) occurs over the hypothesized, obscured unconformity near the top of El Kef A, Core 14. Post-extinction $CaCO_3$ content also remains low in El Kef E up to a depth of ~17.9 mbs. Above this, % $CaCO_3$ values briefly increase to up to ~40 wt% at 17.73 mbs before gradually decreasing back down to lower values (~10 wt%) between 17.73 mbs and 16.15 mbs (Fig. 3E). Above 16.15 mbs, $CaCO_3$ content abruptly increases once more to ~40 wt% and consistently averages around this value up to ~11.5 mbs. $CaCO_3$ declines to ~20 wt% until ~10.08 mbs and then sharply increases to >60 wt% across the unconformity, as at El Kef A.

At the base of El Kef B and C, which are also above the unconformity, % $CaCO_3$ fluctuates at ~55 wt% (Fig. 6D). Above 15.52 mbs in El Kef B, average % $CaCO_3$ values increase to 70 wt% and remain consistently high until the top of the hole. This increase in $CaCO_3$ content occurs meters below the weathering horizon and is also observed at a depth of ~11.5 mbs in El Kef A but is not recorded in El Kef C.

Bulk Organic $\delta^{13}C$

During the earliest part of the Upper Maastrichtian at El Kef (Fig. 3F), $\delta^{13}C_{org}$ values average ~−27.2‰. Between 26.8 mbs and 22.2 mbs in El Kef A, $\delta^{13}C_{org}$ increases by ~1‰. A similar increase is also observed in El Kef E between 27.7 mbs and 22 mbs, but it is more gradual and not as large (~0.5‰), likely because El Kef E was not drilled as deeply as Hole A, so the earliest part of this positive excursion was not recovered. Between 22.2 mbs and 22.0 mbs in El Kef A, $\delta^{13}C_{org}$ values decrease back down to ~–27‰ and remain low until the K/Pg boundary. This same decrease is not observed at a similar depth in El Kef E, where $\delta^{13}C_{org}$ values continue to average ~–26.7‰. At the K/Pg boundary in El Kef A (~20.06 mbs), $\delta^{13}C_{org}$ values are variable (Fig. 3F). However, ~5–20 cm above the boundary, (~19.98–19.8 mbs),

there is a sharp but transient ~0.7‰ increase to average $\delta^{13}C_{org}$ values of −25.9‰, followed by a decrease back to average values of ~–26.5‰. In El Kef E, this positive $\delta^{13}C_{org}$ spike is not observed at the K/ Pg boundary. Instead, there is a ~1‰ transient decrease in $\delta^{13}C_{org}$ between ~19.2 mbs and 19.0 mbs, above which average values return to ~–26.5‰. Following the transient changes in $\delta^{13}C_{org}$ immediately above the K/Pg boundary, bulk organic $\delta^{13}C_{org}$ values are relatively stable until the unconformity at ~17.15 mbs (El Kef A) and ~10.12 mbs (El Kef E), above which there is a 1‰ decrease in $\delta^{13}C_{org}$ (Fig. 3F). The subsequent increase in bulk organic $\delta^{13}C$ above ~9.55 mbs in El Kef E is coincident with the onset of weathering and thus is not considered to be a primary signal.

Above the unconformity at the base of El Kef B, El Kef C (Fig. 6E), and the upper part of El Kef A (Fig. 3F), bulk organic $\delta^{13}C$ values are relatively invariable and remain consistently low (average ~–27.5‰). A slight ~0.5‰ decrease in $\delta^{13}C_{org}$ is observed between 10.2 mbs and 5.47 mbs in El Kef B but not in El Kef A and C. As in El Kef E, the increase to more positive $\delta^{13}C_{org}$ values near the tops of El Kef A, El Kef B, and El Kef C is likely a product of weathering.

Bulk Carbonate $\delta^{13}C$ and $\delta^{18}O$

Throughout the uppermost Maastrichtian at El Kef (~36 mbs-20 mbs in El Kef A, ~28 mbs-18.5 mbs in Hole D, and ~28 mbs-19 mbs in Hole E), bulk carbonate $\delta^{13}C$ gradually increases by 1‰, reaching a maximum of 1.41‰, 1.18‰, and 1.72‰ just below the K/Pg boundary in El Kef A, D, and E, respectively (Fig. 3G). At ~5 cm above the K/Pg boundary, $\delta^{13}C_{carb}$ values abruptly decrease by ~1.4‰. The higher-resolution isotope record of El Kef E shows that this decrease in bulk carbonate δ13C to a minimum value of −2‰ occurs over a ~1 m stratigraphic interval (19.2–18.2 mbs). Two slight $\delta^{13}C_{carb}$ enrichments then occur in El Kef E between 18.2 mbs and 17.5 mbs and between 16.4 mbs and 15.7 mbs (Fig. 3G). However, $\delta^{13}C$ values fluctuate during both depth intervals, making it uncertain whether these transient enrichments reflect any meaningful environmental or stratigraphic changes. Indeed, similar enrichments are not observed at the same depths in Hole D, although the isotope records from this hole are at a much lower resolution than those of Hole E. Above 15.7 mbs in Hole E, $\delta^{13}C_{carb}$ values remain relatively constant, fluctuating around an average value of ~0‰. At ~10.08 mbs in Hole E, bulk carbonate $\delta^{13}C$ increases by ~3‰ (Fig. 3G), which further supports the presence of an unconformity at this depth. Above the unconformity (i.e., from the base to the top of El Kef C; Fig. 6F), bulk carbonate $\delta^{13}C$ gradually increases from ~0.6‰ to 2.5‰ without any major excursions. Overall, we are confident that the trends in our bulk carbonate $\delta^{13}C$ record are predominantly a primary signal, as similar $\delta^{13}C$ values were measured from an overlapping stratigraphic interval in two separate labs (Fig. 3G).

The bulk carbonate $\delta^{18}O$ record for the El Kef cores (Figs. S3 and S4) is variable, with values often fluctuating greatly. This variability is likely the result of diagenetic calcite, which was commonly observed infilling planktic foraminifera tests and has likely over- printed the primary $\delta^{18}O$ signal, as was recently shown in samples from the El Kef GSSP outcrop (Sepúlveda et al., 2019). For this reason, we decided to omit the bulk carbonate $\delta^{18}O$ data from our interpretations. Although the bulk carbonate $\delta^{13}C$ record is likely to have been similarly affected, it is generally more resilient to diagenetic alteration than $\delta^{18}O$ (Margolis et al., 1987). In our $\delta^{13}C$ record, this is supported by the fact that clear paleoenvironmental trends are observed (e.g., at the K/Pg boundary and the unconformity) in concurrence with changes in, e.g., lithology, weight percent $CaCO_3$, and weight percent TOC, which is not the case in the $\delta^{18}O$ record. Furthermore, our bulk carbonate $\delta^{13}C$ record is generally much less variable than our $\delta^{18}O$ record, especially in Hole C (Fig. S4). Nonetheless, although the trends in our $\delta^{13}C$ record

appear to be paleoenvironmentally significant, the absolute $\delta^{13}C$ values should be interpreted with caution, especially when directly comparing to bulk carbonate $\delta^{13}C$ records from other sites, as complex sedimentological, source-related, and diagenetic processes can affect the bulk carbonate $\delta^{13}C$ record (e.g., Minoletti et al., 2005; Sepúlveda et al., 2019).

DISCUSSION

El Kef Composite Section

A composite stratigraphic section ("splice") for the five holes drilled at El Kef was constructed using the biostratigraphic datums, coulometry (weight percent TOC and $CaCO_3$), stable isotopic records, and scanning XRF data (iron [Fe] and zircon [Zr] total counts; Fig. 7). To construct a composite record, the individual cores from each hole were first offset with respect to the drill depth so that prominent features in the data could be correlated. The splice was then defined using the highest-resolution, fullest-coverage data set available within a given stratigraphic interval. The scanning XRF data were therefore particularly critical for constraining the splice, as these data were generated for every core section in each hole and often at a higher resolution and signal-to-noise ratio than the other data types. This meant that general patterns and large-amplitude variations in Fe and Zr (including at the K/Pg boundary) could be finely and reliably matched among cores from different holes. Once the best core sections from parallel holes were spliced together (composite section), offsets were calculated for every core so that the data plotted separately for each individual hole (drilling depth in meters below surface; mbs) could all be plotted on the same depth scale (meters composite depth; mcd).

Overall, our splice represents a stratigraphic record of the entire K/Pg boundary section at El Kef (Fig. 7), including the uppermost Maastrichtian (61.44–78 mcd), the K/Pg extinction horizon (61.44 mcd), the lower Danian (52.5–61.44 mcd), and the mid to upper Danian (0–52.5 mcd). While core correlation is robust in the Upper Maastrichtian and lower Danian (including the K/Pg boundary), the upper Danian section (i.e., in holes B and C) is more challenging to correlate in detail in all records, partly due to the lack of calcareous nannofossil biostratigraphic datums within this interval. Furthermore, intense coring disturbance and weathering can sometimes hinder high-resolution correlation, causing slight mismatches between data from adjacent holes even after applying the offsets. This, coupled with the fact that each of the El Kef holes reveals a structurally complex and distinct stratigraphic succession despite their proximity to one another, makes core correlation challenging. Nevertheless, here we provide a best-possible composite record that reflects the stratigraphic succession recovered from all five holes, which will allow for future integration and fine-tuning of detailed paleontological and geochemical records at El Kef.

Construction of an Age Model: Correlation of the El Kef Composite Core Section to Ocean Drilling Program (ODP) Site 1262 (Walvis Ridge, South Atlantic)

To establish an age model for the El Kef drill cores, we first formed a basic age model based on biostratigraphy. The planktic foraminiferal and nannofossil biostratigraphic datums (Fig. 8; Table 1) do not provide a consistent basis for the Danian part of the record as there are several stratigraphic conflicts between the two taxonomic groups within the El Kef cores (e.g., the FO's of the nannofossil taxa *Coccolithus pelagicus*, *Cruciplacolithus intermedius*, and *Cruciplacolithus tenuis* versus the placement of the P1a, P1b, and P2 planktic foraminiferal datums, respectively; Fig. S2). Thus, we formed one age model using only planktic foraminiferal datums (shown in Table 2) and an alternative age model using only calcareous nannofossil datums (shown in Table 3) for the Danian interval. The K/Pg boundary and base of the Maastrichtian planktic foraminiferal *Plummerita hantkeninoides* biozone were then used to complete the biostratigraphic age model framework. To test both age models and potentially

improve them, we correlated our $\delta^{13}C$ bulk carbonate record, the XRF core scanning Fe elemental data, and biostratigraphic datums (in Tables 2 and 3) to the ODP Site 1262 (Walvis Ridge) record in the equatorial South Atlantic (Figs. 9 and 10), which currently has the best-constrained orbital age model for the latest Cretaceous and early Paleocene (Westerhold et al., 2020). As the Walvis Ridge age model is directly correlated to the Laskar 2010b curve (Laskar et al., 2011), it reports calcareous nannofossil and planktic foraminiferal datums down to three decimal places (i.e., 1000 years). Therefore, in this study, we also report our El Kef biostratigraphic datums down to 1000 years to maintain consistency with the Walvis Ridge age model and to allow for high-precision correlation of the El Kef and Walvis Ridge records. Reducing the precision of the reported ages to one or two decimal places has the potential to introduce artifacts that could be falsely interpreted as phase lags or a delay in the biotic response.

The Upper Maastrichtian part of the El Kef record from the base of the *Plummerita hantkeninoides* biozone (~75.5 mcd) to the K/Pg boundary reveals five well-defined precession-related Fe cycles (Figs. 7B, S5, and S6). This is consistent with a recent study on the K/Pg outcrop section in Zumaia, Spain, which also found five precession cycles (representing ~100 k.y.) between B. *P. hantkeninoides* and the K/Pg boundary (Gilabert et al., 2022). In addition, the Fe cycles in our El Kef cores are correlated to the prominent precession-controlled Fe cycles present at Walvis Ridge (Figs. 9 and 10). Therefore, to provide a more detailed chronology for the Upper Maastrichtian El Kef section, we modified the age model for Site 1262 from Westerhold et al. (2020) for the cycles in the Maastrichtian, assuming they represent precession cycles (Table S1). We then correlated the precession-related cycles for El Kef (Maastrichtian tie Maa1 to Maa5 points 1–5; Table S2; Fig. 7B), aligning maxima in Fe intensity to those at Site 1262. Bulk carbonate $\delta^{13}C$ records confirm this phase relationship (Fig. 11) and the correlation.

Spectral analysis was also attempted for the Paleocene part of the record at El Kef. However, clear cycles were not visible during the earliest Danian (~55–61.5 mcd), and potential ~2 m cyclicity in the XRF Fe data above this (0 to ~55 mcd) cannot be reliably interpreted due to faulting disturbance and uncertainties in the biostratigraphy. This makes the Danian interval at El Kef more challenging to correlate to the Walvis Ridge record. Despite this, we tested two correlation options based on the biostratigraphy (tie points given in Table S2). Our results reveal that the $\delta^{13}C$ bulk carbonate record for El Kef generally shows a much better correlation to the $\delta^{13}C$ bulk carbonate record for Walvis Ridge when using Option 1 (planktic foraminifera-based biostratigraphy; Fig. 11A) than when using Option 2 (calcareous nannofossil-based biostratigraphy; Fig. 11B). Although the magnitude of changes in the $\delta^{13}C$ bulk carbonate record is not expected to be identical at continental shelf/slope sites such as El Kef and pelagic sites such as Walvis Ridge due to the different biogeochemical processes operating in these disparate depositional systems (see Sepúlveda et al., 2019, for detailed discussion), trends in our Option 2 $\delta^{13}C_{carb}$ curve clearly mismatch those in the Walvis Ridge record. This is particularly evident at ca. 65.95 Ma, where the $\delta^{13}C_{carb}$ values in the Walvis Ridge and El Kef Option 1 records continue to decline, whereas $\delta^{13}C_{carb}$ values in the El Kef Option 2 record begin a steady and consistent increase (Fig. 11). A similar increase in $\delta^{13}C_{carb}$ values does not occur until ca. 65.825 Ma in both the Walvis Ridge and the planktic foraminifera-based records, which indicates that the Option 1 correlation is more parsimonious, especially during the earliest Danian.

The higher reliability of the planktic foraminifera-based age model is further revealed in Figure 8. Here, several of the nannofossil datums, especially those from holes A and D, more closely conform to the planktic foraminiferal age-depth plot than the nannofossil age- depth plot, the latter of which is largely based on datums from Hole E. This is puzzling, especially considering that nannofossil biostratigraphy was conducted at much higher resolution in Hole E

than in holes A and D. However, as the earliest Danian succession is thicker in Hole E compared to holes A and D, it is likely that the higher abundance of transitional nannofossil specimens in Hole E made the precise designation of biozone datums within this hole more challenging (see further discussion in the Resolving the Discrepancy between Planktic Foraminiferal and Calcareous Nannofossil Biostratigraphy section).

Taking all of these factors into account, we consider the planktic foraminifera-derived age model (Fig. 9) to be more reliable than the nannofossil-derived age model (Fig. 10). Overall, this preferred age model is robust at and immediately above the K/Pg boundary. However, its reliability decreases during the later Danian (i.e., above the P1b unconformity), where potential tie points such as biostratigraphic datums and geochemical data are scarcer. Although future intensive biostratigraphic and geochemical work will likely improve the resolution of the latter part of the age model, our current composite section still provides a unique record of the K/Pg GSSP, which can be correlated to other sites with orbital age control. This will help to constrain the rate of ecosystem recovery following the K/ Pg mass extinction at El Kef and allow its direct comparison to global sites that sample different depositional environments.

Sedimentation Rates at El Kef

Both our planktic foraminifera- and nannofossil-based age models indicate that the uppermost Maastrichtian is stratigraphically expanded at El Kef, with high sedimentation rates averaging ~11 cm/kyr (Fig. 8). At the K/Pg boundary, the sedimentation rate drops substantially to ~1 cm/ kyr and ~5 cm/kyr in the planktic foraminifera- and nannofossil-based age models, respectively (Fig. 8). In the planktic foraminiferal age model, the sedimentation rate remains consistently at ~1 cm/kyr throughout the rest of the Danian. In contrast, the nannofossil-based age model shows more fluctuation in sedimentation rates, which decline from ~4 cm/kyr to 1 cm/kyr at ~30 k.y. post-impact. Sedimentation rates then increase to up to 7 cm/kyr (at ~250 k.y. post- impact), before declining to ~4 cm/kyr at ~380 k.y. post-impact. Due to differences in the estimated early Danian sedimentation rates in the two models, the unconformity observed in holes D and E (Fig. 4B) occurred either ~1.6 m.y. (planktic foraminiferal age model) or ~0.4 m.y. (calcareous nannofossil age model) after the mass extinction event. When using the favored planktic foraminiferal age model, the duration of the unconformity is estimated to be <500 k.y.

Overall, the higher sedimentation rates predicted by the nannofossil-based age model indicate that the post-extinction sediments in the El Kef cores represent ~1.25 m.y. of the early Paleocene, whereas the planktic foraminifera-based age model suggests that the same depth interval represents >2 m.y. of the Danian. Although sedimentation rates are expected to be relatively high at outer shelf/upper slope sites such as El Kef, the early Danian sedimentation rates of >4 cm/kyr predicted by the nannofossil age model greatly exceed all prior estimates based on the El Kef outcrop section (e.g., Cande and Kent, 1995; Adatte et al., 2002; Stüben et al., 2002). In contrast, the lower Danian sedimentation rates in the planktic foraminifera-based age model are more consistent with previous time-averaged estimates for El Kef (~1.1–2.5 cm/ kyr; Cande and Kent, 1995; Adatte et al., 2002; MacLeod et al., 2018), and with lower estimates for sedimentation rates at nearby Elles, Tunisia (~2–4 cm/kyr; Galeotti et al., 2005), which is more proximal to the shoreline than El Kef and would therefore be expected to have slightly higher sedimentation rates (e.g., Adatte et al., 2002; Stüben et al., 2002; Vellekoop et al., 2015). The fact that sedimentation rates in the calcareous nannofossil-based aged model fluctuate greatly and are much higher than previous estimates for El Kef provides further evidence that the planktic foraminifera-based age model is a more reliable option.

Confounding Issues that Complicate Interpretation of the K/Pg Stratigraphy at El Kef

As mentioned previously, a combination of structural and stratigraphic complexity and drilling disturbance explains several apparent inconsistencies in our composite section and in core correlation, including the different depth levels of the unconformity in holes A, D, and E, and discrepancies in the placement of some planktic foraminiferal biostratigraphic datums between holes along the composite depth scale (e.g., the placement of biozones Pα and P1a in Hole A versus Hole E). Below, we discuss in greater detail how these processes might have impacted our interpretations of the K/Pg stratigraphy at El Kef and the implications.

Structural Complexity

Our multi-hole coring approach has revealed that the K/Pg stratigraphy in the El Kef region is more structurally complex than previously revealed by outcrop studies. This is especially apparent when considering the unique stratigraphic signature of each of the holes. In particular, Hole B recovers a stratigraphic succession that is similar to that of Hole C but different from both the K/Pg GSSP outcrop section (Keller and Lindinger, 1989; Molina et al., 2006) and holes A, D, and E, which are located only ~25 m away (Fig. 2B). Although the K/Pg boundary would likely have been recovered in holes B and C if coring had continued deeper, the K/Pg boundary was present in holes A, D, and E, which were drilled to the same or lesser depths as holes B and C (Figs. 3 and 6). In addition, there are clear local variations in the stratigraphic thickness of the lower Danian successions recovered in holes A, D, and E (Fig. 3), which were drilled within only a few meters of one another (Fig. 2B; Fig. S1). Although it could be argued that cave-in near the inferred unconformity in Hole A (~58.5 mcd; Fig. 7) indicates incomplete core recovery during drilling, there is no similar evidence showing that drilling disturbance also caused differences in the early Danian stratigraphic thicknesses observed in Hole D versus Hole E. For this reason, we suggest a strong tectonic influence (i.e., syn-depositional faulting) on our recovered sediment cores. In particular, we propose a small-offset NW–SE or WNW–ESE normal fault between Hole B and holes A, D, and E that lacks surficial expression due to the argillaceous lithology and thick deposits of Quaternary to recent sediments. This makes the inference of its exact orientation and location imprecise. However, we suggest that this hypothetical fault is in close proximity to holes D and E (due to the particularly intense (micro)fracturing within these holes) and is likely associated with the main fault located ~200 m to the NE of the drill site (Fig. 2). If this fault was active at the time of deposition it would have resulted in an uneven seafloor topography and variable accommodation space that could possibly explain the minor differences in depths to the K-Pg boundary and varied stratigraphic thicknesses of the boundary interval in closely spaced holes A, D, and E. Alternatively, these variations may be a result of a network of microstructures that could have offset the biostratigraphic datums and resulted in thickness differences on a local scale.

Although minor faulting at El Kef has previously been recognized (Negra et al., 2016), evidence for tectonic activity is not readily observed in the outcrop section, which has been described as “free from structural complication.” This was one of the factors that led to its designation as the GSSP for the K/Pg boundary (Molina et al., 2006). However, in our sediment cores, we documented abundant fractures and micro-faults (Figs. 4C–4E), many of which have the NW–SE- dominant trend typical of reactivated regional Late Cretaceous–Paleogene fault systems (Bey et al., 2012; Negra et al., 2016; Fig. 2A). Therefore, it is possible that the weathered marl and shale in the outcrop masks the microstructures that are clearly observed in the cores. This highlights the utility of sediment cores in gaining a deeper and more comprehensive understanding of the underlying geology at a given site, especially those that are designated as reference sections and GSSPs.

Stratigraphic Complexity

The El Kef outcrop, including the GSSP section, preserves what is traditionally thought to be a stratigraphically complete and continuous K/Pg section from the uppermost Maastrichtian to the lower Danian up to planktic foraminiferal biozone P1b (Molina et al., 2006). The biostratigraphic datums and geochemical trends shown in our El Kef composite section are broadly consistent with previous studies of the El Kef outcrop section (e.g., Keller and Lindinger, 1989; Sepúlveda et al., 2019), including a characteristic ~3‰ decrease in $\delta^{13}C_{carb}$ and a sharp decline in weight percent calcium carbonate at the K/Pg boundary (Fig. 7), which is caused by the extinction of >90% of pelagic marine calcifiers (e.g., Bown, 2005; Jiang et al., 2010; Alegret et al., 2012). However, our lithologic and biostratigraphic data indicate an unconformity between ca. 63.98 Ma and 64.40 Ma (based on the planktic foraminifera-derived age model) within planktic foraminiferal zone P1b (e.g., Fig. 4B) that has not previously been recognized in the El Kef outcrop, but which might be related to that recently observed in a nearby outcrop section at Elles, Tunisia (Arenillas et al., 2021).

It is also possible that a second unconformity exists within planktic foraminiferal biozone P1c. This is suggested due to a +~1‰ offset in $\delta^{13}C_{carb}$ values and a +~2‰ offset in $\delta^{13}C_{org}$ values at the top of Hole E compared to the base of Hole C, despite their apparent stratigraphic overlap in the composite section (i.e., between ~49 and 52 mcd; Figs. 7F and 7G). Although the positive $\delta^{13}C_{org}$ excursion at the top of Hole E is likely related to weathering (Fig. 7F), a weathering-induced enrichment of $\delta^{13}C_{carb}$ at the top of Hole E is unlikely and is not observed within the weathered upper cores of any of the other holes (e.g., Hole C; Fig. 7G). In addition, other geochemical parameters (such as the XRF Fe and Zr area counts) that would also be affected by weathering maintain similar values at the top of Hole E versus the base of Hole C and are in fact used in stratigraphic core correlation (Figs. 7B and 7C). Therefore, it is unlikely that the offset in $\delta^{13}C_{carb}$ values between the top of Hole E and base of Hole C can be completely explained by weathering. Alternatively, the presence of a second unconformity and/or faulting activity are plausible explanations for the $\delta^{13}C_{carb}$ discrepancy. Unfortunately, the presence of a second unconformity cannot be confirmed at this time as the top four cores of Hole E were not sampled for planktic foraminifera due to poor preservation. However, a resurgence of intense micro-fracturing within the weathered core tops of holes D and E suggests that syn-depositional faulting was active during this interval and may represent renewed displacement along the previously hypothesized fault (Fig. 2B). Thus, we conclude that the offset between $\delta^{13}C_{carb}$ values at the top of Hole E and the base of Hole C can at least partially be explained by faulting.

Overall, our new data indicate that the K/Pg stratigraphy at El Kef may not be as complete and continuous as previously thought. This has important implications for recently raised questions concerning the completeness of the K/Pg geological record at high time resolution, which might be the cause, at least in part, of the apparent geographic variability of post-extinction fauna (Alegret et al., 2022). As a result, sections traditionally considered to be continuous, such as El Kef, due to the presence of all biozones, may be incomplete in detail and require reevaluation of paleoenvironmental interpretations (Alegret et al., 2022).

Stratigraphic complexity at El Kef is further revealed when comparing our bulk carbonate $\delta^{13}C$ core records to one collected from the El Kef outcrop section (Keller and Lindinger, 1989; Fig. 12). Based on these data, the K/Pg stratigraphy of the outcrop section is most similar to that recorded in our Hole E sediment cores, especially during the lower Danian. Although the early Danian succession in the outcrop section appears thicker than contemporaneous intervals in Hole E, especially during planktic foraminiferal biozones P0 and P1a (Arenillas et al., 2018), this is likely due to different paleontologists conducting the biostratigraphic and taxonomic work on outcrop versus core samples. However, higher up in the

Danian (~2 m above the boundary), the bulk carbonate $\delta^{13}C$ record obtain from the outcrop becomes dissimilar from our Hole E $\delta^{13}C$ data (Fig. 12). Planktic foraminiferal biostratigraphic studies have also yielded contradictory results during this interval (e.g., Keller, 1988a; Keller et al., 1996; Arenillas et al., 2000), potentially because they were conducted on multiple different outcrop sections, although this was poorly documented prior to the official establishment of the "golden spike" GSSP (Molina et al., 2006). Although variations in biostratigraphy can at least partially be explained by the use of differing taxonomic concepts, the dissimilarities in the bulk carbonate $\delta^{13}C$ records of our cores compared to the outcrop section, especially in the later Danian, provide further evidence that the K/Pg stratigraphy at El Kef is locally complex and likely a direct result of the structural complications described previously.

Drilling Disturbance

For holes A, D, and E, which were drilled at approximately the same location (Fig. 2B), the stratigraphic differences between holes can partially be explained by the rotary drilling process. Drilling disturbance and incomplete stratigraphic recovery is particularly likely at and around the lower Danian unconformity at ~52 mcd, which can be recognized by an increase in $\delta^{13}C_{carb}$ and weight percent calcium carbonate, and a decrease in $\delta^{13}C_{org}$ and weight percent TOC (Fig. 7). In Hole E, this lithologic boundary is recognized by a sharp transition from darker- to lighter-colored sediments at ~22 cm in Core 5, with a relatively minor amount of drilling disturbance evident between ~25 cm and 42 cm within the same core (Fig. 4B). In comparison, the same lithologic boundary in Hole D has clearly been more affected by drilling disturbance (Fig. 4B) and is not observed at all in Hole A due to cave-in (Fig. 4I). Drilling disturbance around the unconformity, in the immediate vicinity of the K/Pg boundary (especially in Hole E, Fig. 7) and during other intervals within the El Kef cores; Fig. 4I), often makes the correlation of lithologic features challenging, which leads to irreconcilable inconsistencies in the composite section.

Implications Concerning Designation of El Kef as the K/Pg GSSP

The El Kef outcrop was designated as the GSSP for the K/Pg boundary according to several criteria, including its apparent freedom from structural complication and unconformities (Molina et al., 2006). However, our study provides strong evidence that faulting has had a profound impact on the K/Pg stratigraphy at El Kef and reveals one potentially significant unconformity within planktic foraminiferal biozone P1b. Although these problems do not directly affect the sediments at or below the K/Pg boundary, the stratigraphic signatures of holes A, D, and E start to become disparate less than 1 m above the boundary, which suggests that structural complications begin to affect the sediments within planktic foraminiferal biozone Pα (i.e., within 200–300 Kyr post-impact; Figs. 7 and S2). In addition to the apparent lack of structural complexity, El Kef was also chosen as the K/Pg GSSP due to the "abundance and diversity of well-preserved fossils" (Molina et al., 2006). Although calcareous nannofossils are generally moderately preserved and dinoflagellate cysts are moderately to well-preserved within the Danian at El Kef, planktic foraminifera are often poorly preserved and infilled with secondary carbonate. As well as hampering taxonomic identification for planktic foraminiferal taxonomy, the presence of diagenetic carbonate has also clearly affected our bulk carbonate $\delta^{18}O$ record, and to a lesser extent, our bulk carbonate $\delta^{13}C$ record. As these three data types are typically used in the correlation of stratigraphic sections, the correlation of El Kef to other sections will also likely be challenging as evidenced by our attempted correlation to Walvis Ridge.

Overall, we maintain that our unique composite record from El Kef provides a valuable contribution for better understanding the K/Pg stratigraphy in a global context. However, it is

also a cautionary tale that structural and stratigraphic complications are not always obvious within out- crop sections, especially those composed of shale and marlstone. Therefore, our study reopens previous debates as to whether the El Kef outcrop, with its many challenges, really fulfills the criteria of the K/Pg GSSP, especially given the many auxiliary sections available in Tunisia and the greater Tethys area (Molina et al., 2009).

Resolving the Discrepancy between Planktic Foraminiferal and Calcareous Nannofossil Biostratigraphy

This study highlights significant discrepancies between the early Danian planktic foraminiferal and nannofossil datums at El Kef, the exact reasons for which are difficult to ascertain. Compared to the early Danian calcareous nannofossil biozones, the Paleogene planktic foraminiferal biozones were more recently updated and calibrated to the Geological Time Scale (GTS; Wade et al., 2011), and most of the early Danian marker species are considered to be robust, reliable, and taxonomically easy to identify. Although planktic foraminiferal biozonation schemes continue to be refined and further developed (e.g., Arenillas et al., 2021), the standardized Wade et al. (2011) biozonation scheme is currently widely used within the planktic foraminifera community, which allows for consistency among different studies. In contrast, several alternate nannofossil biozonation schemes continue to be used during the early Danian (e.g., Martini, 1971; Okada and Bukry, 1980; Agnini et al., 2014), none of which has been as precisely calibrated to the GTS (Wade et al., 2011). In addition, each of the nannofossil biozonation schemes suffers from its own specific taxonomic challenge. These challenges are predominantly caused by the presence of abundant "transitional" forms: specimens that represent intermediate morphologies between two closely related species. Transitional forms are particularly common immediately above the K/Pg boundary due to the very high speciation and diversification rates that followed the mass extinction event (Bown et al., 2004) and are more readily observed in relatively stratigraphically expanded sections like El Kef. Although this aspect has exciting implications for examining the evolution of calcareous nannoplankton lineages following the K/Pg mass extinction event in future studies, it makes it challenging to pinpoint potential early Danian biozone marker species that can be consistently and reliably identified taxonomically and morphometrically throughout the nannofossil community.

Within this study, we encountered issues with each of the nannofossil biozonation schemes that we attempted to apply to the El Kef cores. For example, the biozonation schemes of Martini (1971) and Okada and Bukry (1980) rely heavily on the FOs of certain species within the *Cruciplacolithus–Chiasmolithus* lineage. As this lineage evolved very rapidly during the early Danian, there are many transitional forms that likely represent different species or morphotypes, the identification of which has caused controversy and inconsistency in taxonomic concepts for this group (see, e.g., Van Heck and Prins, 1987; Fornaciari et al., 2007; Agnini et al., 2014; and Thibault et al., 2018, for discussion). Taxonomic inconsistencies are particularly troubling when attempting to identify biostratigraphically important *'sensu stricto (s.s.)' Cruciplacolithus/Chiasmolithus* species including *Cr. primus*, *Cr. intermedius*, *Cr. tenuis*, and *Ch. danicus*, all of which are commonly used as biozone markers. Indeed, the taxonomy applied here for most of these species differs from that applied at Site 1262 (Bernaola and Monechi, 2007), and the FOs of the *Cr. primus* and *Cr. intermedius* markers are previously noted as being diachronous (by up to 25–30 k.y.) between Walvis Ridge and Shatsky Rise (Schueth et al., 2015). In addition, at El Kef, we observed many specimens with morphologies that were intermediate between *Cr. primus* and *Cr. intermedius*, and very early forms of probable (but not *s.s.*) *Cr. tenuis* (similar to specimens observed at Bidart, France; Galbrun and Gardin, 2004), which makes it difficult to precisely constrain these datums. The possible evolutionary response

of the *Cruciplacolithus* lineage to ecosystem recovery following the K/ Pg mass extinction events hinders their biostratigraphic utility further (Thibault et al., 2018). The absence of *Cr. tenuis (s.s.)* and *Ch. danicus* at El Kef during a depth interval in which the planktic foraminiferal datums suggest they should be present could be explained if *Cr. tenuis* and *Ch. danicus* originated chronologically later in shelf environmental settings than in pelagic environments as a result of slower nannoplankton recovery at shallower sites (e.g., Thibault et al., 2018; Jones et al., 2019). This hypothesis should be more rigorously tested at other K/Pg sites so that the utility of *Cr. tenuis* and *Ch. danicus* as useful biostratigraphic markers can continue to be critically assessed.

The challenges of using *Cruciplacolithus* species as biostratigraphic markers have been recognized, and an alternate "CNP" biozonation scheme was recommended to resolve these issues (Agnini et al., 2014). However, we also encountered issues when applying this biozonation scheme to the El Kef cores, especially concerning the base common (Bc) *Praeprinsius dimorphosus* group datum (base CNP3), which includes the acme-forming taxa *Praeprinsius tenuiculus*. In the description of this biozone, "common" is defined as "the initial increase in the abundance of this taxon" after which it shows "a continuous presence with abundance values >10 specimens/mm^2" (Agnini et al., 2014). As the method used in Agnini et al. (2014) to quantify the abundance of nannofossils is somewhat user-dependent, we did not apply it here. Therefore, we could not determine the depth at which *Pr. tenuiculus* reached a consistent abundance of >10 specimens/mm^2. However, *Pr. tenuiculus* continues to increase in abundance over several meters of sediment at El Kef and, as with *Cruciplacolithus*, the *Prinsius* lineage experienced rapid evolutionary rates during the early Danian. At El Kef, this is evidenced by the presence of many small, transitional forms with morphologies that are intermediate between *Praeprinsius cf. vegrandis* (the first *Prinsius* species to appear immediately above the K/Pg boundary; Kim, 2020) and *Praeprinsius tenuiculus*. This, coupled with the possibility that *Praeprinsius tenuiculus* may have formed geographically or environmentally asynchronous acmes (Jones et al., 2019), implies that we cannot accurately assign the CNP3 biozone at El Kef. Further taxonomic subjectivity and user-dependency in the designation of other CNP biozones, and significant age deviations for the bases of biozone CNP2 and biozone CNP4, further complicate the application of the Agnini et al. (2014) biozones (Kim, 2020). In fact, Kim (2020) showed that the age discrepancies are substantially less profound when using the traditional nannofossil biozonation model of Martini (1971), which is still pre- dominantly used within the nannofossil community despite its issues during the early Danian.

In summary, the discrepancy between our nannofossil and planktic foraminiferal datums and age models at El Kef is presumably largely a product of taxonomic subjectivity and inconsistency within the commonly used nannofossil biozonation schemes. This is particularly problematic when attempting to correlate datums at two different sites, especially when disparate biozonation schemes or taxonomic concepts are used for each. In contrast, user subjectivity was diminished for our planktic foraminiferal bio- stratigraphy, as the same paleontologist collected these data at both El Kef and Walvis Ridge. In addition to taxonomic inconsistency, it is possible that the FOs of some of the traditional calcareous nannofossil marker species are environmentally controlled, similar to the *Micula prinsii* biozone marker in the Late Maastrichtian (Henriksson, 1993), or possibly impacted by ecological interactions between species (e.g., Schueth et al., 2015), which would call into question their biostratigraphic utility. High-resolution studies from a range of depositional environments and geographic locations are required to critically assess whether this is the case. Finally, our study highlights the role of transitional nannofossil morphologies in complicating interpretations of the K/Pg stratigraphy at

El Kef, but also likely at other stratigraphically expanded early Paleocene sites. As the cores from El Kef contain abundant transitional taxa, we suggest that it as an ideal candidate for conducting detailed morphometric work to better define and constrain the taxonomy of potential early Danian nannofossil markers. This future work would be an important first step in improving and/or developing a calcareous nannofossil biozonation scheme that could be consistently and universally applied to K/Pg sections worldwide.

CONCLUSIONS

The sediment cores recovered from five new holes drilled close to the K/Pg GSSP near El Kef, Tunisia, provide over 100 m of unweathered, accessible material for future high-resolution analyses. Our new composite section and age model, based on correlation of the XRF Fe, bulk carbonate $\delta^{13}C$, and biostratigraphic data to the orbitally tuned Walvis Ridge record, confirm that the El Kef cores are stratigraphically expanded relative to other contemporaneous sections. More importantly, we reveal that these new cores preserve an apparently continuous record of the last ~250 k.y. of the Maastrichtian, the K/Pg boundary itself, and the earliest Danian (planktic foraminiferal biozones P0 to P2; ~3.5 m.y. post-extinction), except for a < 500-k.y.-long unconformity near the top of Danian planktic foraminiferal biozone P1b (~1.6 m.y. post-impact). Overall, we consider our El Kef age model to be robust for the Upper Maastrichtian as the cores preserve precessional orbital rhythms that allow a high-resolution time scale to be constructed. Although these orbital cycles are not as prominent during the Danian, the planktic foraminiferal biozone datums below the inferred unconformity at ~52 mcd are well- constrained, leading to reasonable correlation of the El Kef and Walvis Ridge records and thus a relatively reliable age model. However, the age model becomes less reliable above the P1b unconformity as there is only one planktic foraminiferal datum as a tie point and geochemical data are scarcer. Thus, we urge caution when interpreting results above the unconformity on a time scale.

Another challenge in constructing the Danian part of the age model, and one of the most significant findings of our study, is the influence of tectonic processes on the local stratigraphy at El Kef. This is exemplified by the fact that two of the cored sections (holes B and C), which were drilled within 75 m of the other three sections (holes A, D, and E), preserve a different stratigraphic portion of the lower Danian. Moreover, holes A, D, and E each show different depths to the K/Pg boundary and P1b unconformity, as well as variable stratigraphic thicknesses of the earliest Danian interval. These differences are likely a result of syn-depositional faulting that resulted in uneven seafloor topography. In addition, many of the microstructural features revealed within our El Kef cores were not observed in outcrop, which indicates that a combination of sediment core and outcrop data should be used to gain a more comprehensive understanding of the stratigraphy of this site, especially considering its designation as a GSSP. Despite these caveats, and the attendant challenges in core correlation, the age model contained herein is far more detailed and complete than existing models based on the El Kef outcrop, and it can be used to reliably place paleoceanographic, paleoenvironmental, and paleoecological work on the K/ Pg boundary GSSP into a global context.

ACKNOWLEDGMENTS

We thank Thomas Frederichs, University of Bremen, Germany, for his attempted paleomagnetic analyses on the El Kef cores and Marwa Baroumi for her assistance in the field during both drilling seasons. Drilling and core shipment was supported by NASA Exobiology NNX12AD83G (to T. Bralower). H. Birch acknowledges support from the European Research Council grant PAst Links in the Evolution of Ocean's Global ENvIronment and Ecology (PA-LEOGENiE). J. Sepúlveda acknowledges support from the Massachusetts Institute of Technology International Science and Technology Initiative (MIT- MISTI Spain) Seed Grant,

the University of Colorado Boulder, and National Science Foundation awards 2037750 and 2021648. J. Vellekoop acknowledges support from the Research Foundation Flanders (FWO) grant 12Z6618N. J.H. Whiteside acknowledges financial support from the Annual Adventures in Research award and Megan Wilding and Bastian Hambach for laboratory assistance. L. Alegret acknowledges support from grant PID2019-105537RB- I00 funded by MCIN/AEI/10.13039/501100011033 and by "ERDF A way of making Europe," and the Government of Aragon (Reference Group E33_17R). M. Henehan acknowledges financial support from the Yale Peabody Museum and laboratory assistance from Jule Hoysagk. J.v. Dijk acknowledges financial support from the Swiss National Science Foundation. Funded by the Deutsche Forschungsgemeinschaft (DFG, German Research Foundation) under Germany's Excellence Strategy – EXC-2077-390741603 ("The Ocean Floor–Earth's Uncharted Interface," research unit RECORDER). Last (but not least), we thank Philippe Claeys and another anonymous reviewer for their helpful comments and suggestions, which helped to greatly improve the quality of this manuscript.

REFERENCES CITED

Adatte, T., Keller, G., and Stinnesbeck, W., 2002, Late Cretaceous to early Paleocene climate and sea-level fluctuations: The Tunisian record: Palaeogeography, Palaeoclimatology, Palaeoecology, v. 178, p. 165–196, https://doi.org/10.1016/S0031-0182(01)00395-9.

Agnini, C., Fornaciari, E., Raffi, I., Catanzariti, R., Pälike, H., Backman, J., and Rio, D., 2014, Biozonation and bio- chronology of Paleogene calcareous nannofossils from low and middle latitudes: Newsletters on Stratigraphy, v. 47, p. 131–181, https://doi.org/10.1127/0078-0421/2014/0042.

Alegret, L., 2003, Sedimentologíay micropaleontología (foraminíferos bentónicos) del tránsito Cretácico–Terciario: Correlación entrelas áreas del Golfo de México y del Tethys [Ph.D. thesis]: Zaragoza, España, Universitarias de Zaragoza, 476 p.

Alegret, L., 2008, Evolución paleoambiental durante el tránsito Cretácico/Paleógeno basada en foraminíferos bentónicos: Revista Española de Paleontología, v. 23, p. 15–30.

Alegret, L., Arenillas, I., Arz, J.A., Díaz, C., Grajales- Nishimura, J.M., Meléndez, A., Molina, E., Rojas, R., and Soria, A.R., 2005, Cretaceous–Paleogene boundary deposits at Loma Capiro, central Cuba: Evidence for the Chicxulub impact: Geology, v. 33, p. 721–724, https://doi.org/10.1130/G21573.1.

Alegret, L., Thomas, E., and Lohmann, K.C., 2012, End-Cretaceous marine mass extinction not caused by productivity collapse: Proceedings of the National Academy of Sciences of the United States of America, v. 109, p. 728–732, https://doi.org/10.1073/pnas.1110601109.

Alegret, L., Arreguín-Rodríguez, G.J., and Thomas, E., 2022, Oceanic productivity after the Cretaceous/Paleogene impact: Where do we stand? The view from the deep, in Koeberl, C., Claeys, P., and Montanari, A., eds., From the Guajira Desert to the Apennines, and from Mediterranean Microplates to the Mexican Killer Asteroid: Geological Society of America Special Paper 557, https://doi.org/10.1130/2022.2557(21).

Alvarez, L.W., Alvarez, W., Asaro, F., and Michel, H.V., 1980, Extraterrestrial cause for the Cretaceous–Tertiary extinction: Science, v. 208, p. 1095–1108, https://doi.org/10.1126/science.208.4448.1095.

Arenillas, I., Arz, J.A., Molina, E., and Dupuis, C., 2000, An independent test of planktic foraminiferal turnover across the Cretaceous/Paleogene (K/P) boundary at El Kef, Tunisia; catastrophic mass extinction and possible survivorship: Micropaleontology, v. 46, p. 31–49.

Arenillas, I., Arz, J., and Molina, E., 2004, A new high-resolution planktic foraminiferal zonation and subzonation for the lower Danian: Lethaia, v. 37, p. 79–95, https:// doi.org/10.1080/00241160310005097.
Arenillas, I., Arz, J.A., Grajales-Nishimura, J.M., Murillo- Muñetón, G., Alvarez, W., Camargo-Zanoguera, A., Molina, E., and Rosales-Domínguez, C., 2006, Chicxulub impact event is Cretaceous/Paleogene boundary in age: New micropaleontological evidence: Earth and Planetary Science Letters, v. 249, p. 241–257, https:// doi.org/10.1016/j.epsl.2006.07.020.
Arenillas, I., Arz, J.A., and Gilabert, V., 2018, Blooms of ab- errant planktic foraminifera across the K/Pg boundary in the Western Tethys: Causes and evolutionary implications: Paleobiology, v. 44, p. 460–489, https://doi.org/10.1017/pab.2018.16.
Arenillas, I., Gilabert, V., and Arz, J.A., 2021, New bio- chronological scales of planktic foraminifera for the early Danian based on high-resolution biostratigraphy: Geosciences, v. 11, p. 479, https://doi.org/10.3390/geosciences11110479.
Bernaola, G., and Monechi, S., 2007, Calcareous nannofossil extinction and survivorship across the Cretaceous−Paleogene boundary at Walvis Ridge (ODP Hole 1262C, South Atlantic Ocean): Palaeogeography, Palaeoclimatology, Palaeoecology, v. 255, p. 132–156, https://doi.org/10.1016/j.palaeo.2007.02.045.
Bey, S., Kuss, J., Silva, I.P., Negra, M.H., and Gardin, S., 2012, Fault-controlled stratigraphy of the Late Cretaceous Abiod Formation at Ain Medheker (Northeast Tunisia): Cretaceous Research, v. 34, p. 10–25, https:// doi.org/10.1016/j.cretres.2011.09.008.
Birch, H.S., Coxall, H.K., Pearson, P.N., Kroon, D., and Schmidt, D.N., 2016, Partial collapse of the marine carbon pump after the Cretaceous–Paleogene boundary: Geology, v. 44, p. 287–290, https://doi.org/10.1130/G37581.1.
Bouaziz, S., Barrier, E., Soussi, M., Turki, M.M., and Zouari, H., 2002, Tectonic evolution of the northern African margin in Tunisia from paleostress data and sedimentary record: Tectonophysics, v. 357, p. 227–253, https:// doi.org/10.1016/S0040-1951(02)00370-0.
Bourgeois, J., Hansen, T.A., Wiberg, P.L., and Kauffman, E.G., 1988, A tsunami deposit at the Cretaceous–Tertiary boundary in Texas: Science, v. 241, p. 567–570, https://doi.org/10.1126/science.241.4865.567.
Bown, P., 2005, Selective calcareous nannoplankton survivorship at the Cretaceous–Tertiary boundary: Geology, v. 33, p. 653–656, https://doi.org/10.1130/G21566AR.1.
Bown, P.R., Lees, J.A., and Young, J.R., 2004, Calcareous nannoplankton evolution and diversity through time, in Thierstein, H.R., and Young, J.R., eds., Coccolithophores: From Molecular Processes to Global Impact: Berlin, Heidelberg, Springer, p. 481–508, https://doi.org/10.1007/978-3-662-06278-4_18.
Bralower, T.J., Paull, C.K., and Mark Leckie, R., 1998, The Cretaceous–Tertiary boundary cocktail: Chicxulub impact triggers margin collapse and extensive sediment gravity flows: Geology, v. 26, p. 331–334, https://doi.org/10.1130/0091-7613(1998)026<0331:TCTBCC>2.3.CO;2.
Brinkhuis, H., and Zachariasse, W.J., 1988, Dinoflagellate cysts, sea level changes and planktonic foraminifers across the Cretaceous–Tertiary boundary at El Haria, northwest Tunisia: Marine Micropaleontology, v. 13, p. 153–191, https://doi.org/10.1016/0377-8398(88)90002-3.
Brinkhuis, H., Bujak, J.P., Smit, J., Versteegh, G.J.M., and Visscher, H., 1998, Dinoflagellate-based sea surface temperature reconstruction across the Cretaceous– Tertiary boundary:

Palaeogeography, Palaeoclimatology, Palaeoecology, v. 141, p. 67–83, https://doi.org/10.1016/S0031-0182(98)00004-2.
Brönnimann, P., 1952, Globigerinidae from the Upper Cretaceous (Cenomanian–Maastrichtian) of Trinidad: Bulletins of American Paleontology, v. 34, p. 1–71.
Buffetaut, E., 1990, Vertebrate extinctions and survival across the Cretaceous–Tertiary boundary: Tectonophysics, v. 171, p. 337–345, https://doi.org/10.1016/0040-1951(90)90108-K.
Burollet, P.F., 1956, Contribution à L'étude Stratigraphique de la Tunisie Centrale, Annales des Mines et de la Geologie, Vol. 18: Tunis, La Rapide, 350 p.
Burollet, P.F., 1967, General geology of Tunisia, in Martin, L., ed., Guidebook to the Geology and History of Tunisia: Tripoli, Petroleum Exploration Society of Libya, p. 51–58.
Cande, S.C., and Kent, D.V., 1995, Revised calibration of the geomagnetic polarity timescale for the Late Cretaceous and Cenozoic: Journal of Geophysical Research: Solid Earth, v. 100, p. 6093–6095, https://doi.org/10.1029/94JB03098.
Claeys, P., Kiessling, W., and Alvarez, W., 2002, Distribution of Chicxulub ejecta at the Cretaceous–Tertiary boundary, in Koeberl, C., and MacLeod, K.G., eds., Catastrophic Events and Mass Extinctions: Impacts and Beyond: Geological Society of America Special Paper 356, p. 55–68, https://doi.org/10.1130/0-8137-2356-6.55.
Coccioni, R., and Premoli Silva, I., 2015, Revised Upper Albian–Maastrichtian planktonic foraminiferal biostratigraphy and magnetostratigraphy of the classical Tethyan Gubbio section (Italy): Newsletters on Stratigraphy, v. 48, p. 47–90, https://doi.org/10.1127/nos/2015/0055.
Coxall, H.K., D'Hondt, S., and Zachos, J.C., 2006, Pelagic evolution and environmental recovery after the Cretaceous–Paleogene mass extinction: Geology, v. 34, p. 297–300, https://doi.org/10.1130/G21702.1.
Dinarès-Turell, J., Westerhold, T., Pujalte, V., Röhl, U., and Kroon, D., 2014, Astronomical calibration of the Danian stage (Early Paleocene) revisited: Settling chronologies of sedimentary records across the Atlantic and Pacific Oceans: Earth and Planetary Science Letters, v. 405, p. 119–131, https://doi.org/10.1016/j.epsl.2014.08.027.
D'Hondt, S., Pilson, M.E., Sigurdsson, H., Hanson, A.K., Jr., and Carey, S., 1994, Surface-water acidification and extinction at the Cretaceous–Tertiary boundary: Geology, v. 22, p. 983–986, https://doi.org/10.1130/0091-7613(1994)022<0983:SWAAEA>2.3.CO;2.
D'Hondt, S., Donaghay, P., Zachos, J.C., Luttenberg, D., and Lindinger, M., 1998, Organic carbon fluxes and ecological recovery from the Cretaceous–Tertiary mass extinction: Science, v. 282, p. 276–279, https://doi.org/10.1126/science.282.5387.276.
Donze, P., Colin, J.P., Damotte, R., Oertli, H.J., Peypouquet, J.P., and Said, R., 1982, Les ostracodes du Campanien terminal à l'Eocene infèrieur de la coupe du Kef, Tunisie Nord-occidentale: Bulletin des Centres de Recherches Exploration–Production Elf–Aquitaine, v. 6, p. 173–335.
Fornaciari, E., Giusberti, L., Luciani, V., Tateo, F., Agnini, C., Backman, J., Oddone, M., and Rio, D., 2007, An expanded Cretaceous–Tertiary transition in a pelagic setting of the Southern Alps (central-western Tethys): Palaeogeography, Palaeoclimatology, Palaeoecology, v. 255, p. 98–131, https://doi.org/10.1016/j.palaeo.2007.02.044.
Galbrun, B., and Gardin, S., 2004, New chronostratigraphy of the Cretaceous–Paleogene boundary interval at Bidart (France): Earth and Planetary Science Letters, v. 224, p. 19–32, https://doi.org/10.1016/j.epsl.2004.04.043.

1313 Galeotti, S., Brinkhuis, H., and Huber, M., 2004, Records of post-Cretaceous–Tertiary boundary
1314 millennial-scale cooling from the western Tethys: A smoking gun for the impact-winter
1315 hypothesis?: Geology, v. 32, p. 529–532, https://doi.org/10.1130/G20439.1.
1316 Galeotti, S., et al., 2005, Orbitally paced cycles from the lowermost Danian Elles section
1317 (Tunisia): Implications for high-resolution chronostratigraphy across the
1318 Cretaceous/Tertiary boundary: European Geosciences Union General Assembly (Vienna,
1319 April 24–29, 2005): Geophysical Research Abstract 06425.
1320 Gilabert, V., Batenburg, S.J., Arenillas, I., and Arz, J.A., 2022, Contribution of orbital forcing
1321 and Deccan volcanism to global climatic and biotic changes across the Cretaceous–
1322 Paleogene boundary at Zumaia, Spain: Geology, v. 50, p. 21–25,
1323 https://doi.org/10.1130/G49214.1.
1324 Giron, M.M.-T., 2013, Establishing geochemical constraints on mass accumulation rates across
1325 the Cretaceous– Paleogene boundary with extraterrestrial Helium-3 [M.S. thesis]:
1326 Cambridge, Massachusetts Institute of Technology, 75 p.
1327 Goolaerts, S., Kennedy, W.J., Dupuis, C., and Steurbaut, E., 2004, Terminal Maastrichtian
1328 ammonites from the Cretaceous–Paleogene Global Stratotype Section and Point, El Kef,
1329 Tunisia: Cretaceous Research, v. 25, p. 313–328,
1330 https://doi.org/10.1016/j.cretres.2004.01.002.
1331 Goto, K., et al., 2008, Lateral lithological and compositional variations of the
1332 Cretaceous/Tertiary deep-sea tsunami deposits in northwestern Cuba: Cretaceous
1333 Research, v. 29, p. 217–236, https://doi.org/10.1016/j.cretres.2007.04.004.
1334 Gradstein, F.M., Ogg, J.G., Schmitz, M.D., and Ogg, G.M., eds., 2012, The Geological Time
1335 Scale 2012: Amsterdam, Elsevier, 1176 p.
1336 Gulick, S.P., et al., 2019, The first day of the Cenozoic: Proceedings of the National Academy of
1337 Sciences of the United States of America, v. 116, p. 19,342–19,351,
1338 https://doi.org/10.1073/pnas.1909479116.
1339 Henehan, M.J., et al., 2019, Rapid ocean acidification and protracted Earth system recovery
1340 followed the end-Cretaceous Chicxulub impact: Proceedings of the National Academy of
1341 Sciences of the United States of America, v. 116, p. 22,500–22,504,
1342 https://doi.org/10.1073/pnas.1905989116.
1343 Henriksson, A.S., 1993, Biochronology of the terminal Cretaceous calcareous nannofossil Zone
1344 of Micula prinsii: Cretaceous Research, v. 14, p. 59–68,
1345 https://doi.org/10.1006/cres.1993.1005.
1346 Hull, P.M., et al., 2020, On impact and volcanism across the Cretaceous–Paleogene boundary:
1347 Science, v. 367, p. 266–272, https://doi.org/10.1126/science.aay5055.
1348 Jablonski, D., 1991, Extinctions: A paleontological perspective: Science, v. 253, p. 754–757,
1349 https://doi.org/10.1126/science.253.5021.754.
1350 Jablonski, D., 1994, Extinctions in the fossil record: Philosophical Transactions of the Royal
1351 Society of London B: Biological Sciences, v. 344, p. 11–17,
1352 https://doi.org/10.1098/rstb.1994.0045.
1353 Jiang, S., Bralower, T.J., Patzkowsky, M.E., Kump, L.R., and Schueth, J.D., 2010, Geographic
1354 controls on nannoplankton extinction across the Cretaceous/Palaeogene boundary: Nature
1355 Geoscience, v. 3, p. 280–285, https:// doi.org/10.1038/ngeo775.
1356 Jones, H.L., Lowery, C.M., and Bralower, T.J., 2019, Delayed calcareous nannoplankton boom-
1357 bust successions in the earliest Paleocene Chicxulub (Mexico) impact crater: Geology, v.
1358 47, p. 753–756, https://doi.org/10.1130/G46143.1.

1359 Kadri, A., Essid, E.M., and Merzeraud, G., 2015, “Kasserine Island” boundaries variations
1360 during the Upper Cretaceous–Eocene (central Tunisia): Journal of African Earth
1361 Sciences, v. 111, p. 244–257, https://doi.org/10.1016/j.jafrearsci.2015.07.027.
1362 Kaiho, K., Oshima, N., Adachi, K., Adachi, Y., Mizukami, T., Fujibayashi, M., and Saito, R.,
1363 2016, Global climate change driven by soot at the K-Pg boundary as the cause of the
1364 mass extinction: Scientific Reports, v. 6, p. 1–13, https://doi.org/10.1038/srep28427.
1365 Karoui-Yaakoub, N., Zaghbib-Turki, D., and Keller, G., 2002, The Cretaceous–Tertiary (K–T)
1366 mass extinction in planktic foraminifera at Elles I and El Melah, Tunisia:
1367 Palaeogeography, Palaeoclimatology, Palaeoecology, v. 178, p. 233–255,
1368 https://doi.org/10.1016/S0031-0182(01)00398-4.
1369 Keller, G., 1988a, Extinction, survivorship and evolution of planktic foraminifera across the
1370 Cretaceous/Tertiary boundary at El Kef, Tunisia: Marine Micropaleontology, v. 13, p.
1371 239–263, https://doi.org/10.1016/0377-8398(88)90005-9.
1372 Keller, G., 1988b, Biotic turnover in benthic foraminifera across the Cretaceous/Tertiary
1373 boundary at El Kef, Tunisia: Palaeogeography, Palaeoclimatology, Palaeoecology, v. 66,
1374 p. 153–171, https://doi.org/10.1016/0031-0182(88)90198-8.
1375 Keller, G., 1992, Paleoecologic response of Tethyan benthic foraminifera to the Cretaceous–
1376 Tertiary boundary transition, in Takayanagi, Y., and Saito, T., eds., Studies in Benthic
1377 Foraminifera: Tokyo, Tokai University Press, p. 77–91.
1378 Keller, G., 2004, Low-diversity, late Maastrichtian and early Danian planktic foraminiferal
1379 assemblages of the eastern Tethys: Journal of Foraminiferal Research, v. 34, p. 49–73,
1380 https://doi.org/10.2113/0340049.
1381 Keller, G., and Lindinger, M., 1989, Stable isotope, TOC and CaCO3 record across the
1382 Cretaceous/Tertiary boundary at El Kef, Tunisia: Palaeogeography, Palaeoclimatology,
1383 Palaeoecology, v. 73, p. 243–265, https://doi.org/10.1016/0031-0182(89)90007-2.
1384 Keller, G., Li, L., and MacLeod, N., 1996, The Cretaceous/Tertiary boundary stratotype section
1385 at El Kef, Tunisia: How catastrophic was the mass extinction?: Palaeogeography,
1386 Palaeoclimatology, Palaeoecology, v. 119, p. 221–254, https://doi.org/10.1016/0031-
1387 0182(95)00009-7.
1388 Keller, G., Adatte, T., Stinnesbeck, W., Luciani, V., Karoui-Yaakoub, N., and Zaghbib-Turki,
1389 D., 2002, Paleoecology of the Cretaceous–Tertiary mass extinction in planktonic
1390 foraminifera: Palaeogeography, Palaeoclimatology, Palaeoecology, v. 178, p. 257–297,
1391 https://doi.org/10.1016/S0031-0182(01)00399-6.
1392 Kim, H., 2020, The Paleocene radiation of calcareous nannoplankton [Ph.D thesis]: London,
1393 University College London, 218 p.
1394 Kuslys, M., and Krähenbühl, U., 1983, Noble metals in Cretaceous/Tertiary sediments from El
1395 Kef: Radiochimica Acta, v. 34, p. 139–142, https://doi.org/10.1524/ract.1983.34.3.139.
1396 Laskar, J., Fienga, A., Gastineau, M., and Manche, H., 2011, La2010: A new orbital solution for
1397 the long-term motion of the Earth: Astronomy & Astrophysics, v. 532, A89,
1398 https://doi.org/10.1051/0004-6361/201116836.
1399 Lindinger, M., 1988, The Cretaceous/Tertiary boundaries of El Kef and Caravaca:
1400 Sedimentological, geochemical and clay mineralogical aspects [Ph.D. thesis]: Zürich,
1401 ETH Zurich, 253 p.
1402 Lowery, C.M., et al., 2018, Rapid recovery of life at ground zero of the end-Cretaceous mass
1403 extinction: Nature,v. 558, p. 288–291, https://doi.org/10.1038/s41586-018-0163-6.

Lowery, C.M., et al., 2021, Early Paleocene paleoceanography and export productivity in the Chicxulub crater: Paleoceanography and Paleoclimatology, v. 36, https://doi.org/10.1029/2021PA004241.
MacLeod, K.G., Quinton, P.C., Sepúlveda, J., and Negra, M.H., 2018, Postimpact earliest Paleogene warming shown by fish debris oxygen isotopes (El Kef, Tunisia): Science, v. 360, p. 1467–1469, https://doi.org/10.1126/science.aap8525.
Margolis, S.V., Mount, J.F., Doehne, E., Showers, W., and Ward, P., 1987, The Cretaceous/Tertiary boundary carbon and oxygen isotope stratigraphy, diagenesis, and paleoceanography at Zumaya, Spain: Paleoceanography, v. 2, p. 361–377, https://doi.org/10.1029/PA002i004p00361.
Marshall, C.R., and Ward, P.D., 1996, Sudden and gradual molluscan extinctions in the latest Cretaceous of western European Tethys: Science, v. 274, p. 1360–1363, https://doi.org/10.1126/science.274.5291.1360.
Martini, E., 1971, Standard Tertiary and Quaternary calcareous nannoplankton zonation, in Proceedings, Second International Conference of Planktonic Microfossils, Roma, Italy 1970, Volume 2: Tecnoscienza, p. 739–785.
Méon, H., 1990, Palynologic studies of the Cretaceous–Tertiary boundary interval at El Kef outcrop, northwestern Tunisia: Paleogeographic implications: Review of Palaeobotany and Palynology, v. 65, p. 85–94, https://doi.org/10.1016/0034-6667(90)90059-R.
Minoletti, F., De Rafélis, M., Renard, M., Gardin, S., and Young, J., 2005, Changes in the pelagic fine fraction carbonate sedimentation during the Cretaceous–Paleocene transition: Contribution of the separation technique to the study of Bidart section: Palaeogeography, Palaeoclimatology, Palaeoecology, v. 216, p. 119–137, https://doi.org/10.1016/j.palaeo.2004.10.006.
Molina, E., Alegret, L., Arenillas, I., Arz, J.A., Gallala, N., Hardenbol, J., Salis, K.V., Steurbaut, E., Vandenberghe, N., and Zaghbib-Turki, D., 2006, The global boundary stratotype section and point for the base of the Danian stage (Paleocene, Paleogene," Tertiary," Cenozoic) at El Kef, Tunisia-original definition and revision: Episodes,v. 29, p. 263–273, https://doi.org/10.18814/epiiugs/2006/v29i4/004.
Molina, E., Alegret, L., Arenillas, I., Arz, J.A., Gallala, N., Grajales-Nishimura, J.M., Murillo-Muñetón, G., and Zaghbib-Turki, D., 2009, The global boundary stratotype section and point for the base of the Danian stage (Paleocene, Paleogene," Tertiary", Cenozoic): auxiliary sections and correlation: Episodes, v. 32, p. 84–95, https://doi.org/10.18814/epiiugs/2009/v32i2/002.
Negra, M.H., 1994, Les dépôts de plate-forme à bassin du Crétacé supérieur en Tunisie centro-septentrionale. Sédimentation et Diagenèse des series du Crétacé supérieur (formation Abiod et faciès associés). Stratigraphie, Sédimentation, Diagenèse et Intérêt pétrolier [Ph.D. thesis]: Tunis, Université de Tunis, 548 p.
Negra, M.H., and Jaballah, J., 2020, The rudist-rich carbonate units in central Tunisia as markers of Late Cretaceous transgressive events: Arabian Journal of Geosciences, v. 13, p. 1–16, https://doi.org/10.1007/ s12517-020-06354-y.
Negra, M.H., Skelton, P.W., Gili, E., Valldeperas, F.X., and Argles, T., 2016, Recognition of massive Upper Cretaceous carbonate bodies as olistoliths using rudist bivalves as internal bedding indicators (Campanian Merfeg Formation, Central Tunisia): Cretaceous Research, v. 66, p. 177–193, https://doi.org/10.1016/j.cretres.2016.06.003.

Norris, R.D., Huber, B.T., and Self-Trail, J., 1999, Synchroneity of the KT oceanic mass extinction and meteorite impact: Blake Nose, western North Atlantic: Geology, v. 27, p. 419–422, https://doi.org/10.1130/0091-7613(1999)027<0419:SOTKTO>2.3.CO;2.

Ocampo, A.C., Pope, K.O., and Fischer, A.G., 1996, Ejecta blanket deposits of the Chicxulub crater from Albion Island, Belize, in Ryder, G., Fastovsky, D.E., and Gartner, S., eds., The Cretaceous-Tertiary Event and Other Catastrophes in Earth History: Geological Society of America Special Paper 307, p. 75–88, https://doi.org/10.1130/0-8137-2307-8.75.

Ohno, S., et al., 2014, Production of sulphate-rich vapour during the Chicxulub impact and implications for ocean acidification: Nature Geoscience, v. 7, p. 279–282, https://doi.org/10.1038/ngeo2095.

Okada, H., and Bukry, D., 1980, Supplementary modification and introduction of code numbers to the low-latitude coccolith biostratigraphy (Bukry, 1973, 1975): Marine Micropaleontology, v. 5, p. 321–325, https://doi.org/10.1016/0377-8398(80)90016-X.

Olsson, R.K., Berggren, W.A., Hemleben, C., and Huber, B.T., 1999, Atlas of Paleocene Planktonic Foraminifera: Washington D.C., Smithsonian Institution Press, 252 p., https://doi.org/10.5479/si.00810266.85.1.

Pardo, A., Ortiz, N., and Keller, G., 1996, Latest Maastrichtian and Cretaceous–Tertiary boundary foraminiferal turnover and environmental changes at Agost, Spain, in MacLeod, N., and Keller, G., eds., The Cretaceous/Tertiary Boundary Mass Extinction: Biotic and Environmental Events: New York, Norton Press, p. 139–171.

Perch-Nielsen, K., McKenzie, J., and He, Q., 1982, Biostratigraphy and isotope stratigraphy and the 'catastrophic' extinction of calcareous nannoplankton at the Cretaceous/Tertiary boundary, in Silver, L.T., and Schultz, P.H., eds., Geological Implications of Impacts of Large Asteroids and Comets on the Earth: Geological Society of America Special Paper 190, p. 353–372, https://doi.org/10.1130/SPE190-p353.

Peypouquet, J.P., Grousset, F., and Mourguiart, P., 1986, Paleooceanography of the Mesogean Sea based on ostracods of the northern Tunisian continental shelf between the Late Cretaceous and early Paleogene: Geologische Rundschau, v. 75, p. 159–174, https://doi.org/10.1007/BF01770185.

Pospichal, J.J., 1994, Calcareous nannofossils at the KT boundary, El Kef: No evidence for stepwise, gradual, or sequential extinctions: Geology, v. 22, p. 99–102, https://doi.org/10.1130/0091-7613(1994)022<0099:CNATKT>2.3.CO;2.

Rasmussen, J.A., Heinberg, C., and Håkansson, E., 2005, Planktonic foraminifers, biostratigraphy and the diachronous nature of the lowermost Danian Cerithium Limestone at Stevns Klint, Denmark: Bulletin of the Geological Society of Denmark, v. 52, p. 113–131, https://doi.org/10.37570/bgsd-2005-52-09.

Robin, E., and Rocchia, R., 1998, Ni-rich spinel at the Cretaceous–Tertiary boundary of El Kef, Tunisia: Bulletin de la Société Géologique de France, v. 169, p. 365–372.

Robin, E., Boclet, D., Bonté, P., Froget, L., Jéhanno, C., and Rocchia, R., 1991, The stratigraphic distribution of Ni-rich spinels in Cretaceous–Tertiary boundary rocks at El Kef (Tunisia), Caravaca (Spain) and hole 761C (Leg 122): Earth and Planetary Science Letters, v. 107, no. 3–4, p. 715–721, https://doi.org/10.1016/0012-821X(91)90113-V.

Rodríguez-Tovar, F.J., Uchman, A., M'Hamdi, A., Riahi, S., and Ismail-Lattrache, K.B., 2016, Ichnological record of palaeoenvironment from the Cretaceous–Paleogene boundary interval at El Kef, Tunisia: The first study of old and new sections at the stratotype area:

Journal of African Earth Sciences, v. 120, p. 23–30, https://doi.org/10.1016/j.jafrearsci.2016.04.017.
Rosenberg, Y.O., Ashckenazi-Polivoda, S., Abramovich, S., Thibault, N., Chin, S., Feinstein, S., Bartov, Y., and Amrani, A., 2021, Resilience of primary and export productivity in a eutrophic ecosystem following the Cretaceous–Paleogene mass extinction: Global and Planetary Change, v. 196, https://doi.org/10.1016/j.gloplacha.2020.103371.
Salaj, J., 1974, Preposition pour les hypostratotypes du Danien et du Paléocen (Localité type de formation El Haria: Le Kef, Tunisie eptentrionale): Notes du Service Géologique de Tunisie, v. 41, p. 1–14.
Salaj, J., 1980, Microbiostratigraphie du Crétacé et du Paleéogène de la Tunisie septentrionale et orien- tale (Hypostratotypes tunisiens): Bratislava, Institut Géologique de Dionyz Stûra, 238 p.
Schueth, J.D., Bralower, T.J., Jiang, S., and Patzkowsky, M.E., 2015, The role of regional survivor incumbency in the evolutionary recovery of calcareous nannoplankton from the Cretaceous/Paleogene (K/Pg) mass extinction: Paleobiology, v. 41, p. 661–679, https://doi.org/10.1017/pab.2015.28.
Schulte, P., et al., 2010, The Chicxulub asteroid impact and mass extinction at the Cretaceous–Paleogene boundary: Science, v. 327, p. 1214–1218, https://doi.org/10.1126/science.1177265.
Schulte, P., Smit, J.A.N., Deutsch, A., Salge, T., Friese, A., and Beichel, K., 2012, Tsunami backwash deposits with Chicxulub impact ejecta and dinosaur remains from the Cretaceous–Palaeogene boundary in the La Popa Basin, Mexico: Sedimentology, v. 59, p. 737–765, https://doi.org/10.1111/j.1365-3091.2011.01274.x.
Scotese, C.R., 2001, PALEOMAP Project: http://www.scotese.com (accessed July 2021).
Sepúlveda, J., Wendler, J.E., Summons, R.E., and Hinrichs, K.U., 2009, Rapid resurgence of marine productivity after the Cretaceous–Paleogene mass extinction: Science, v. 326, p. 129–132, https://doi.org/10.1126/science.1176233.
Sepúlveda, J., Alegret, L., Thomas, E., Haddad, E., Cao, C., and Summons, R.E., 2019, Stable isotope constraints on marine productivity across the Cretaceous–Paleogene mass extinction: Paleoceanography and Paleoclimatology, v. 34, p. 1195–1217, https://doi.org/10.1029/2018PA003442.
Sheehan, P.M., and Fastovsky, D.E., 1992, Major extinctions of land-dwelling vertebrates at the Cretaceous–Tertiary boundary, eastern Montana: Geology, v. 20, p. 556–560, https://doi.org/10.1130/0091-7613(1992)020<0556:MEOLDV>2.3.CO;2.
Sigurdsson, H., D'Hondt, S., Arthur, M.A., Bralower, T.J., Zachos, J.C., Van Fossen, M., and Channel, J.E., 1991, Glass from the Cretaceous/Tertiary boundary in Haiti: Nature, v. 349, p. 482–487, https://doi.org/10.1038/349482a0.
Smit, J., 1982, Extinction and evolution of planktonic foraminifera after a major impact at the Cretaceous/Tertiary boundary, in Silver, L.T., and Schultz, P.H., eds., Geological Implications of Impacts of Large Asteroids and Comets on the Earth, Geological Society of America Special Paper 190, p. 329–352, https://doi.org/10.1130/SPE190-p329.
Smit, J., 1999, The global stratigraphy of the Cretaceous– Tertiary boundary impact ejecta: Annual Review of Earth and Planetary Sciences, v. 27, p. 75–113, https:// doi.org/10.1146/annurev.earth.27.1.75.
Smit, J., and Romein, A.J.T., 1985, A sequence of events across the Cretaceous–Tertiary boundary: Earth and Planetary Science Letters, v. 74, p. 155–170, https:// doi.org/10.1016/0012-821X(85)90019-6.

Smit, J., and Ten Kate, W.G.H.Z., 1982, Trace-element patterns at the Cretaceous–Tertiary boundary—consequences of a large impact: Cretaceous Research, v. 3, p. 307–332, https://doi.org/10.1016/0195-6671(82)90031-3.

Smit, J., Montanari, A., Swinburne, N.H., Alvarez, W., Hildebrand, A.R., Margolis, S.V., Claeys, P., Lowrie, W., and Asaro, F., 1992, Tektite-bearing, deep-water clastic unit at the Cretaceous–Tertiary boundary in northeastern Mexico: Geology, v. 20, p. 99–103, https://doi.org/10.1130/0091-7613(1992)020<0099:TBDWCU>2.3.CO;2.

Smit, J., Roep, T.B., Claeys, P., Grajales-Nishimura, J.M., and Bermudez, J., 1996, Coarse-grained, clastic sandstone complex at the K/T boundary around the Gulf of Mexico: Deposition by tsunami waves, in Ryder, G., Fastovsky, D.E., and Gartner, S., eds., The Cretaceous–Tertiary Event and Other Catastrophes in Earth History: Geological Society of America Special Paper 307, p. 151–182, https://doi.org/10.1130/0-8137-2307-8.151.

Speijer, R.P., and Van der Zwaan, G.J., 1996, Extinction and survivorship of Southern Tethyan benthic foraminifera across the Cretaceous/Paleogene boundary, in Hart, M.B., ed., Biotic Recovery from Mass Extinction Events: Geological Society of London Special Publication 102, p. 343–371, https://doi.org/10.1144/GSL.SP.1996.001.01.26.

Strong, C.P., 2000, Cretaceous-Tertiary foraminiferal succession at Flaxbourne River, Marlborough, New Zealand: New Zealand Journal of Geology and Geophysics, v. 43, p. 1–20, https://doi.org/10.1080/00288306.2000.9514867.

Stüben, D., Kramar, U., Berner, Z., Stinnesbeck, W., Keller, G., and Adatte, T., 2002, Trace elements, stable isotopes, and clay mineralogy of the Elles II K–T boundary section in Tunisia: Indications for sea level fluctuations and primary productivity: Palaeogeography, Palaeoclimatology, Palaeoecology, v. 178, p. 321–345, https://doi.org/10.1016/S0031-0182(01)00401-1.

Thibault, N., Galbrun, B., Gardin, S., Minoletti, F., and Le Callonnec, L., 2016, The end-Cretaceous in the southwestern Tethys (Elles, Tunisia): Orbital calibration of paleoenvironmental events before the mass extinction: International Journal of Earth Sciences, v. 105, p. 771– 795, https://doi.org/10.1007/s00531-015-1192-0.

Thibault, N., Minoletti, F., and Gardin, S., 2018, Offsets in the early Danian recovery phase in carbon isotopes: Evidence from the biometrics and phylogeny of the Cruciplacolithus lineage: Revue de Micropaleontologie, v. 61, p. 207–221, https://doi.org/10.1016/j.revmic.2018.09.002.

Urrutia-Fucugauchi, J., Marin, L., and Trejo-Garcia, A., 1996, UNAM scientific drilling program of Chicxulub impact structure—evidence for a 300 kilometer crater diameter: Geophysical Research Letters, v. 23, p. 1565– 1568, https://doi.org/10.1029/96GL01566.

Van Heck, S.E., and Prins, B., 1987, A refined nannoplankton zonation for the Danian of the Central North Sea: Abhandlungen der Geologischen Bundesanstalt, v. 39,p. 285–303.

Vellekoop, J., Sluijs, A., Smit, J., Schouten, S., Weijers, J.W., Damsté, J.S.S., and Brinkhuis, H., 2014, Rapid short- term cooling following the Chicxulub impact at the Cretaceous–Paleogene boundary: Proceedings of the National Academy of Sciences, v. 111, p. 7537–7541, https://doi.org/10.1073/pnas.1319253111.

Vellekoop, J., Smit, J., van de Schootbrugge, B., Weijers, J.W., Galeotti, S., Damste, J.S.S., and Brinkhuis, H., 2015, Palynological evidence for prolonged cooling along the Tunisian continental shelf following the K– Pg boundary impact: Palaeogeography, Palaeoclimatology, Palaeoecology, v. 426, p. 216–228, https://doi.org/10.1016/j.palaeo.2015.03.021.

Vellekoop, J., Esmeray-Senlet, S., Miller, K.G., Browning, J.V., Sluijs, A., van de Schootbrugge, B., Sinninghe Damsté, J.S., and Brinkhuis, H., 2016, Evidence for Cretaceous–Paleogene boundary bolide "impact winter" conditions from New Jersey, USA: Geology, v. 44, p. 619–622, https://doi.org/10.1130/G37961.1.

Verbeek, J.W., 1977, Calcareous nannoplankton biostratigraphy of Middle and Upper Cretaceous deposits in Tunisia, Southern Spain and France: Utrecht Micropaleontological Bulletin, v. 16, p. 1–157.

Vonhof, H.B., and Smit, J., 1997, High-resolution late Maastrichtian–early Danian oceanic 87Sr/86Sr record: Implications for Cretaceous-Tertiary boundary events: Geology, v. 25, p. 347–350, https://doi.org/10.1130/0091-7613(1997)025<0347:HRLMED>2.3.CO;2.

Wade, B.S., Pearson, P.N., Berggren, W.A., and Pälike, H.,2011, Review and revision of Cenozoic tropical planktonic foraminiferal biostratigraphy and calibration to the geomagnetic polarity and astronomical time scale: Earth-Science Reviews, v. 104, p. 111–142, https://doi.org/10.1016/j.earscirev.2010.09.003.

Westerhold, T., et al., 2020, An astronomically dated record of Earth's climate and its predictability over the last 66 million years: Science, v. 369, p. 1383–1387, https://doi.org/10.1126/science.aba6853.

Zachos, J.C., and Arthur, M.A., 1986, Paleoceanography of the Cretaceous/Tertiary boundary event: Inferences from stable isotopic and other data: Paleoceanography, v. 1, p. 5–26, https://doi .org /10 .1029 /PA001i001p00005.

Zaghbib-Turki, D., Karoui-Yaakoub, N., Said-Benzarti, R., Rocchia, R., and Robin, E., 2001, Révision de la limite Crétacé-Tertiaire de la coupe d'Ellès (Tunisie): Proposition d'un nouveau parastratotype: Geobios, v. 34, p. 25–37, https://doi.org/10.1016/S0016-6995(01)80040-1.

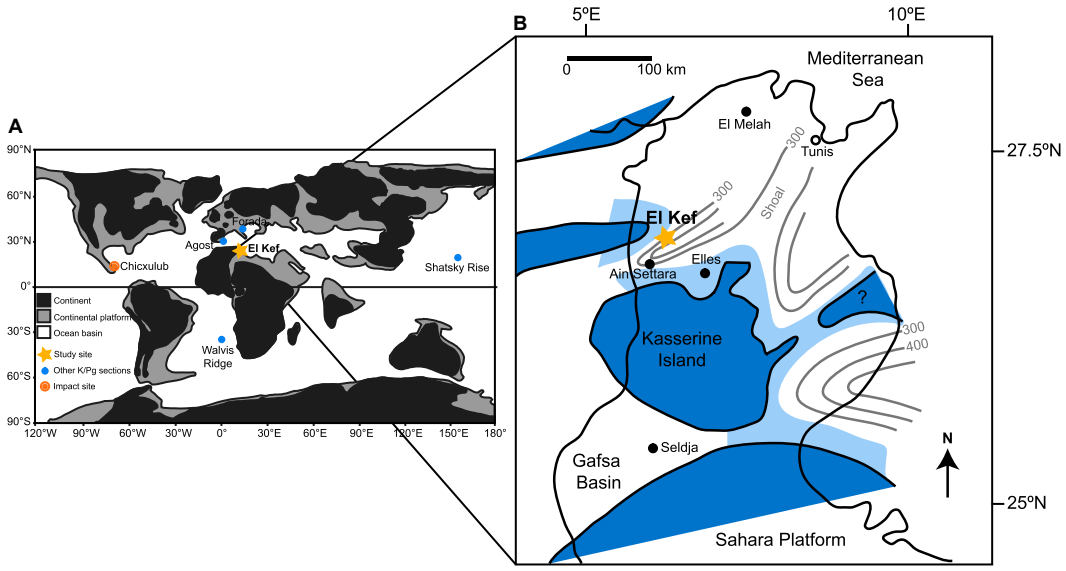

Figure 1. (A) Paleogeographic map of the Late Maastrichtian to early Paleogene created using PALEOMAP (Scotese, 2001) shows the location of the El Kef section in relation to other K/Pg sites. (B) Simplified paleogeographic map of northwestern Tunisia during the Late Maastrichtian to early Danian shows the depositional setting of the El Kef section (star) and other Tunisian K/Pg sections (modified after Burollet, 1967). Isolines indicate depth in meters. Paleogeographic coordinates are estimated following Alegret (2003)

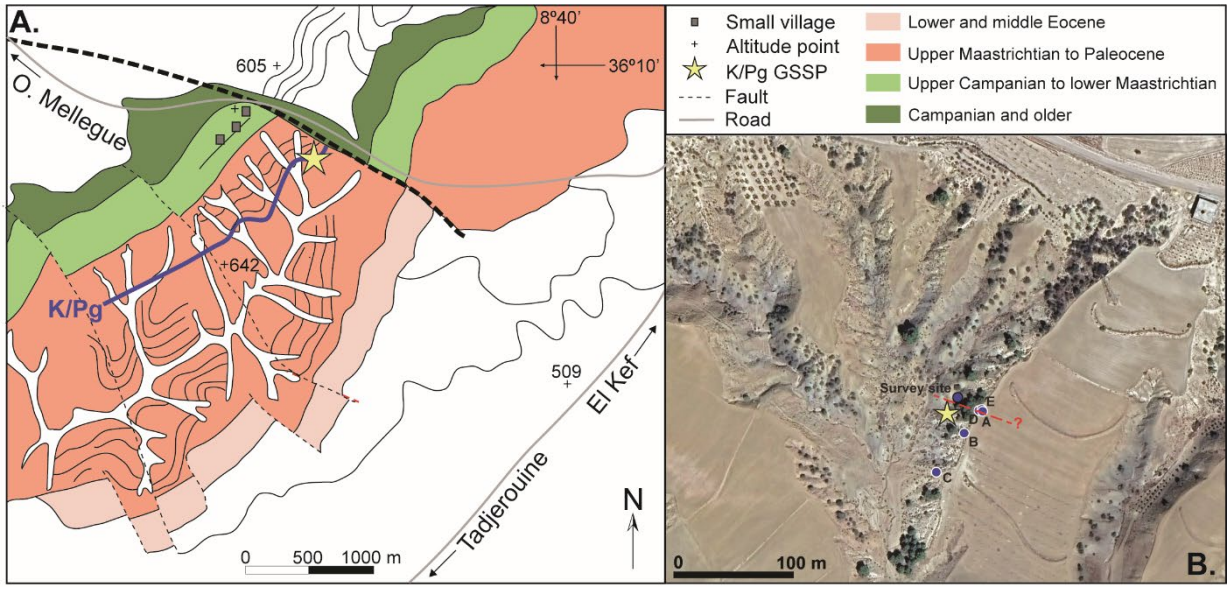

Figure 2. (A) Location of the K/Pg Global Stratigraphic Section and Point (GSSP) outcrop section (yellow star) within context of the regional geology (modified from Lindinger, 1988) shows NW–SE to NNW–SSE faults that appear to have impacted sedimentation. The major fault that runs along and approximately parallel to the closest road (northern part of map) is represented by a thicker black dashed line. The red box indicates the area shown in Figure 2B. (B) Google Earth map image shows the exact location of the holes drilled during the El Kef Coring Program in relation to the GSSP outcrop section (yellow star) and the new auxiliary outcrop section that was used to guide drilling (labeled "Survey site"; MacLeod et al., 2018). A possible minor fault between Hole B and holes A, D, and E is shown as a red dashed line. A more detailed Google Earth map is shown in Figure S1

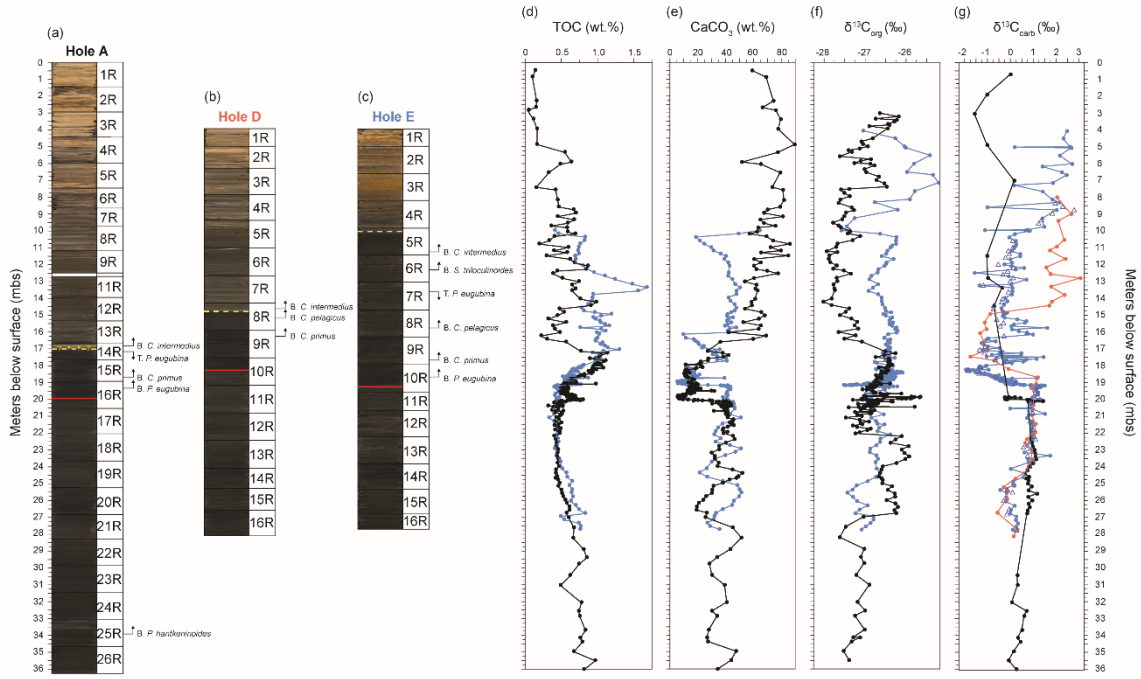

Figure 3. Line-scan images are shown for (A) El Kef Hole A, (B) El Kef Hole D, and (C) El Kef Hole E with core numbers and key planktic foraminiferal and calcareous nannofossil datums to the right of each image. The relative position of the K/Pg boundary as determined biostratigraphically in each hole is shown by a red line, and the relative position of the unconformity in each hole is shown by a yellow dashed line. Associated geochemical data from El Kef A (black lines), El Kef Hole D (orange lines), and El Kef Hole E (blue lines) are shown in panels D through G. (D) Weight percent total organic carbon (TOC), (E) weight percent calcium carbonate ($CaCO_3$), (F) bulk organic $\delta^{13}C$, and (G) bulk carbonate $\delta^{13}C$. The dark blue open triangles in panel G indicate additional stable isotope data that were collected at Yale University, New Haven, Connecticut, USA; all other data in this panel were collected at the National Oceanography Centre, University of Southampton, UK. Data are plotted against meters below surface (mbs), which explains the mismatch in data between holes.

(A) K/Pg boundary

El Kef A 16R-1A

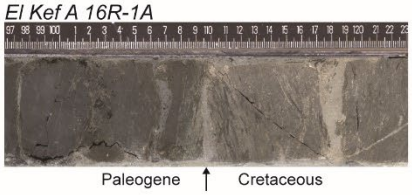

Paleogene ↑ Cretaceous

El Kef D 10R-1A

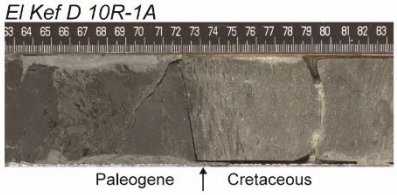

Paleogene ↑ Cretaceous

El Kef E 10R-1A

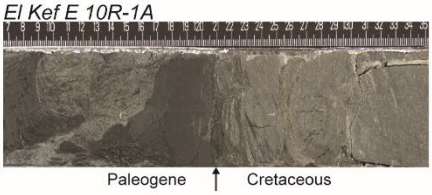

Paleogene ↑ Cretaceous

(B) Unconformity

El Kef D 8R-1A

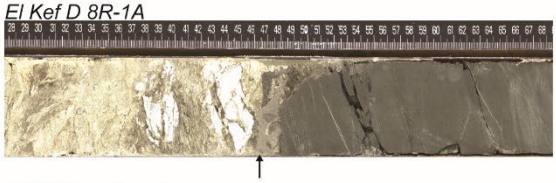

El Kef E 5R-1A

(C) Microfractures

El Kef E 9R-1A

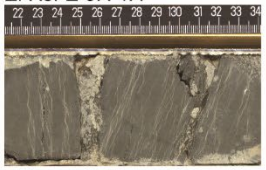

El Kef C 21R-1A

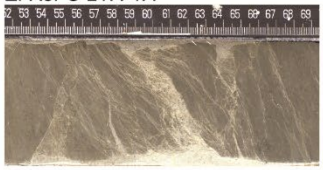

(D) Fractures

El Kef E 6R-1A

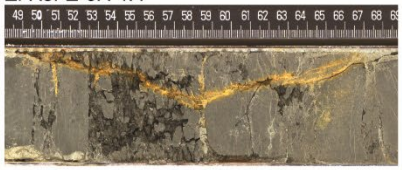

El Kef B 18R-1A

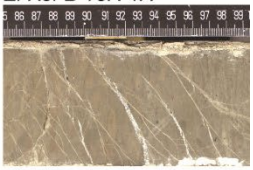

(E) Microfaulting

*El Kef A 12R-1A**

(F) Weathering

*El Kef E 2R-1A**

(G) Bioturbation

El Kef A 18R-1A

El Kef B 13R-1A

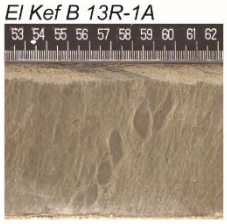

El Kef B 18R-1A

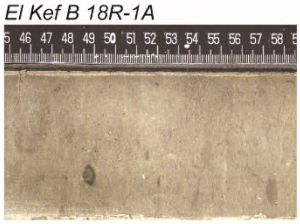

El Kef B 8R-1A

(H) Laminations

El Kef B 11R-1A

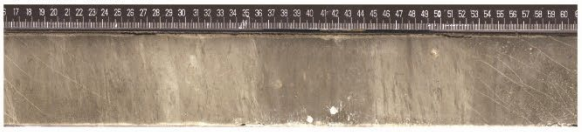

*El Kef C 11R-1A**

(I) Drilling disturbance

*El Kef A 13R-1A**

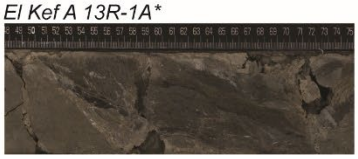

*El Kef A 14R-1A** – Cave-in

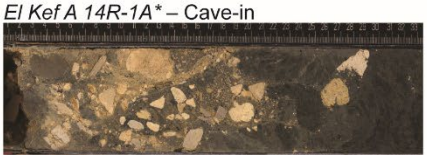

El Kef B 23R-1A – Drill biscuits

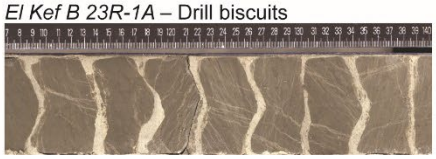

Figure 4. Line-scan images show important lithostratigraphic features within the El Kef cores. Most of the core images shown were taken with a 6.7× aperture, as these camera settings generally made the desired features and structures on the split-core surfaces more visible. Core sections denoted with an asterisk (*) indicate images taken with an 11× aperture. (A) The K/Pg boundary in holes A, D and E, marked by a sharp transition from lighter-gray marl (uppermost Maastrichtian) to darker-gray marl (lowermost Paleocene). Boundary is located with arrow. (B) The upper P1b unconformity in holes D and E, as evidenced by a sharp transition from darker-gray (older) to lighter-gray (younger) marl. Also note the drilling disturbance immediately above and below the unconformity in Hole D and below the unconformity in Hole E. (C) Representative examples of the severe microfracturing that occurs within restricted stratigraphic intervals. (D) Examples of larger fractures that are infilled by partially oxidized material (left) and by a white crystalline mineral (likely sparry calcite cement; right). (E) Infilled micro-fault within Hole A showing clear displacement of sediment on either side of the contact. (F) Representative example of the weathering/oxidization of sediments within the top two to three cores from each hole. This alteration often obscures structural features on the split-core surfaces. (G) Examples of bioturbated sediments from the uppermost Maastrichtian (left-most image) and from within Danian planktic foraminiferal biozones P1c-P2 (remaining images). Burrows are rare immediately above the K/Pg boundary, but gradually increase in abundance and diversity throughout the lower Danian. Also note the pyrite-lined burrow at approximately 49 cm in Hole B 18R-1A. (H) Examples of (sub)-parallel laminations (left) and low- to higher-angle cross laminations (right). (I) Evidence of drilling disturbance within the sediment cores. The “cave-in” shown in the middle image, whereby younger material falls into the hole during drilling, likely obscures the unconformity within Hole A. Biscuiting (right-hand image), which is caused by drilling fluid flowing into the sediment cracks formed during rotary drilling, is common throughout the El Kef cores.

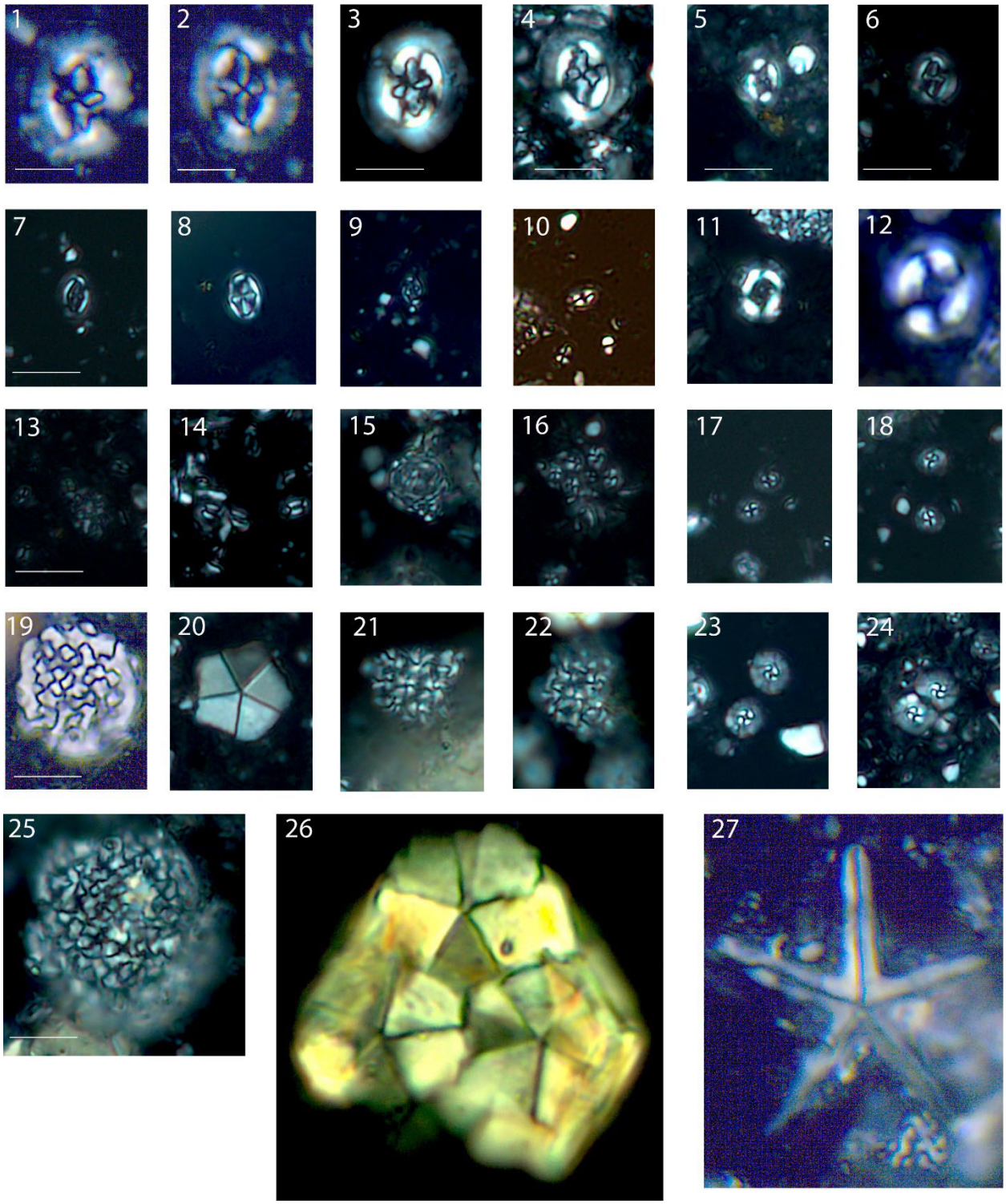
1
2
3
4
5
6
7
8
9
10
11
12
13
14
15
16
17
18
19
20
21
22
23
24
25
26
27

Figure 5. Common calcareous nannofossil taxa observed in the El Kef cores are shown. (1, 2) *Cruciplacolithus "pretenuis",* 1. Hole C-7R-1, 61 cm; 2. Hole C-3R-1, 1 cm. (3, 4) *Cruciplacolithus intermedius*, 3. Hole C-2R-1, 100 cm; 4. Hole C-5R-1, 10 cm. (5–9) *Cruciplacolithus primus*, 5. Hole E-9R-1, 30 cm; 6. Hole E, 4R-1, 50 cm; 7. Hole E, 5R-1, 30 cm; 8. Hole E, 8R-1, 130 cm (early morphotype); 9. Hole E, 8R-1, 90 cm (early morphotype). (10–12) *Coccolithus pelagicus*, 10. Hole E, 7R-1, 149 cm (early morphotype); 11. Hole E, 9R-1, 50 cm; 12. Hole D, 8R-1, 60 cm. (13–15) *Neobiscutum parvulum*, 13. Hole E, 5R-1, 110 cm; 14. Hole E, 6R-1, 110 cm; 15. Hole E, 8R-1, 10 cm (coccosphere). (16–18) *Praeprinsius cf. vegrandis*, 16. Hole E, 4R-1, 50 cm; 17. Hole E, 4R-1, 50 cm; 18. Hole E, 4R-1, 50 cm. (19, 25) *Cervisiella* spp., 19. Hole A, 15R-1, 29 cm; 25. Hole E, 8R-1, 10 cm. (20, 26) *Braarudosphaera bigelowii*. 20. Hole E, 8R-1, 10 cm; 26. Hole E, 10R-1, 10 cm. (21–22) *Futyania petalosa*, 21. Hole E, 4R-1, 50 cm; 22. Hole E, 4R-1, 50 cm. (23, 24) *Prinsius tenuiculus*, 23. Hole C, 3R-1, 20 cm; 24. Hole C, 4R-1, 16 cm. (27) *Micrantholithus cf. entaster*. 27. Hole C, 23R-1, 147 cm. Scale bars are 5 μm, and all images are at the same scale except for 1 and 2, which are slightly less enlarged than the other images.

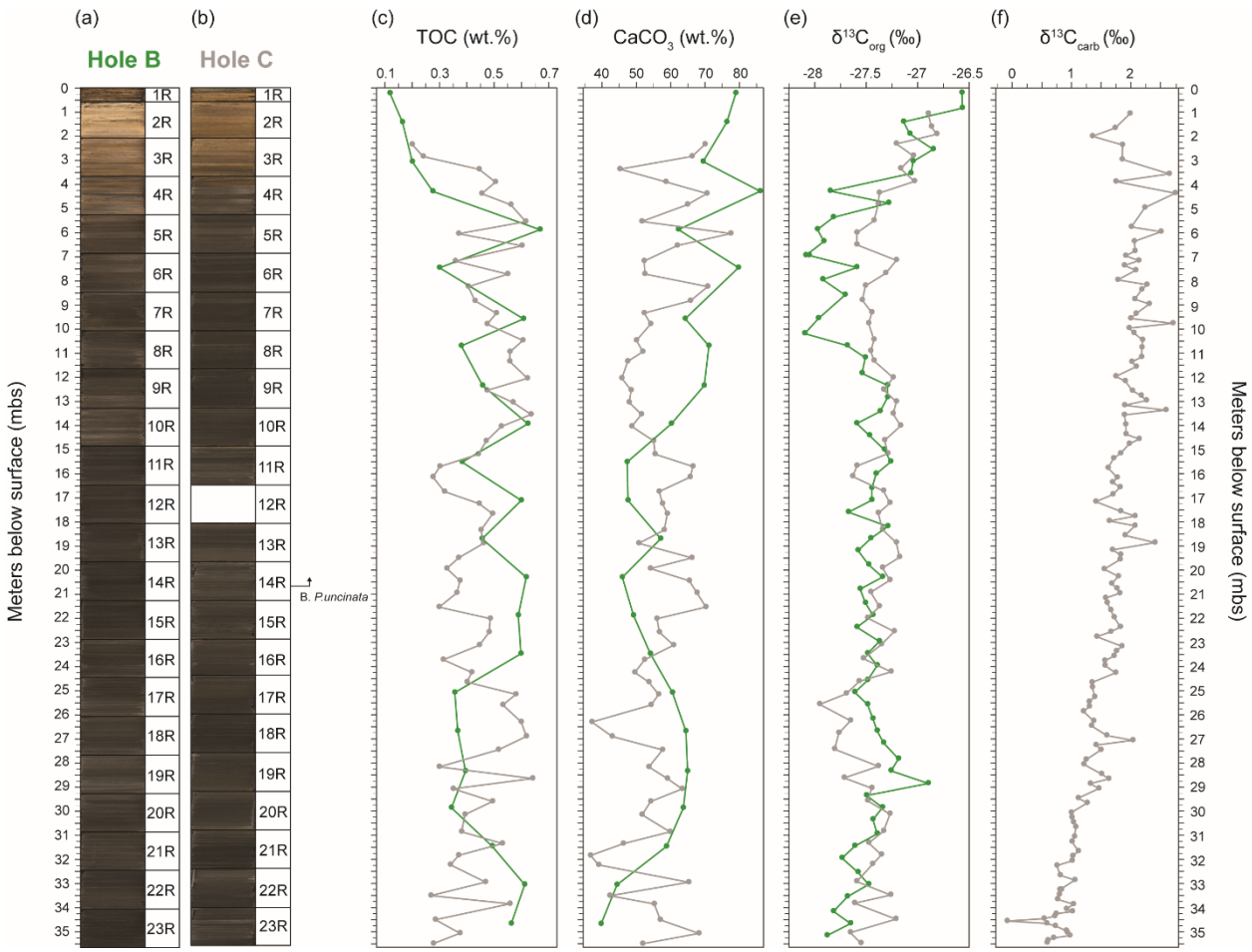

Figure 6. Line-scan images for (A) El Kef Hole B and (B) El Kef Hole C, with core numbers shown to the right of each hole. The *Praemurica uncinata* planktic foraminiferal datum is also displayed next to panel B. Panels C through F show associated geochemical data from El Kef Hole B (green lines) and El Kef Hole C (gray lines). (C) Weight percent total organic carbon (TOC), (D) weight percent calcium carbonate ($CaCO_3$), (E) bulk organic $\delta^{13}C$, and (F) bulk carbonate $\delta^{13}C$. Data are plotted against meters below surface (mbs) for each hole.

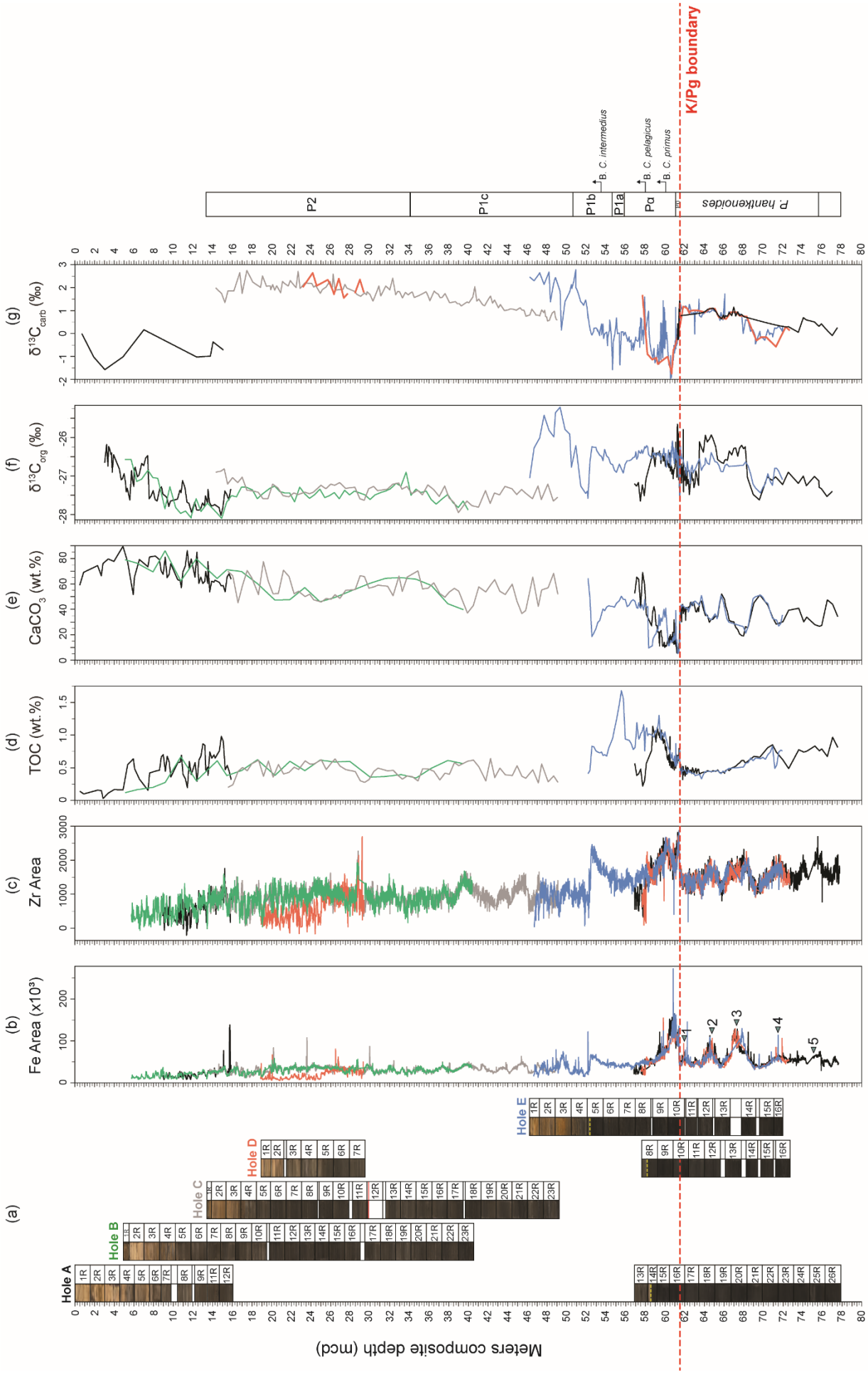
(a)
(b) Fe Area (x10³)
(c) Zr Area
(d) TOC (wt.%)
(e) CaCO3 (wt.%)
(f) δ13Corg (‰)
(g) δ13Ccarb (‰)
Meters composite depth (mcd)
Hole A
Hole B
Hole C
Hole D
Hole E
P2
P1c
P1b
P1a
Pα
P. hantkenoides
B. C. intermedius
B. C. pelagicus
B. C. primus
K/Pg boundary
1
2
3
4
5

Figure 7. Composite section derived from the splice for El Kef is shown. The K/Pg boundary is marked by the red dashed line. (A) Line-scan images for El Kef A to El Kef E, with core numbers to the right of the images. The white spaces between core images signify stratigraphic gaps. The yellow dashed lines in holes A, D, and E represent the inferred position of the unconformity based on lithological, biostratigraphic, and geochemical observations. Panels B through G show the compiled geochemical data colored by hole: El Kef Hole A (black), El Kef Hole B (green), El Kef Hole C (gray), El Kef Hole D (orange), and El Kef Hole E (blue). (B) Iron (Fe) X-ray fluorescence (XRF) data, with numbered arrows marking the Maastrichtian precessional cycles as defined by spectral analysis (Figs. S5 and S6), (C) zircon (Zr) XRF data, (D) weight percent total organic carbon (TOC), (E) weight percent calcium carbonate ($CaCO_3$), (F) bulk organic $\delta^{13}C$, and (G) bulk carbonate $\delta^{13}C$. The right-hand side of the figure shows the planktic foraminiferal biozones from Hole E. Nannofossil datums (based on the Hole E biostratigraphy) are shown to the right.

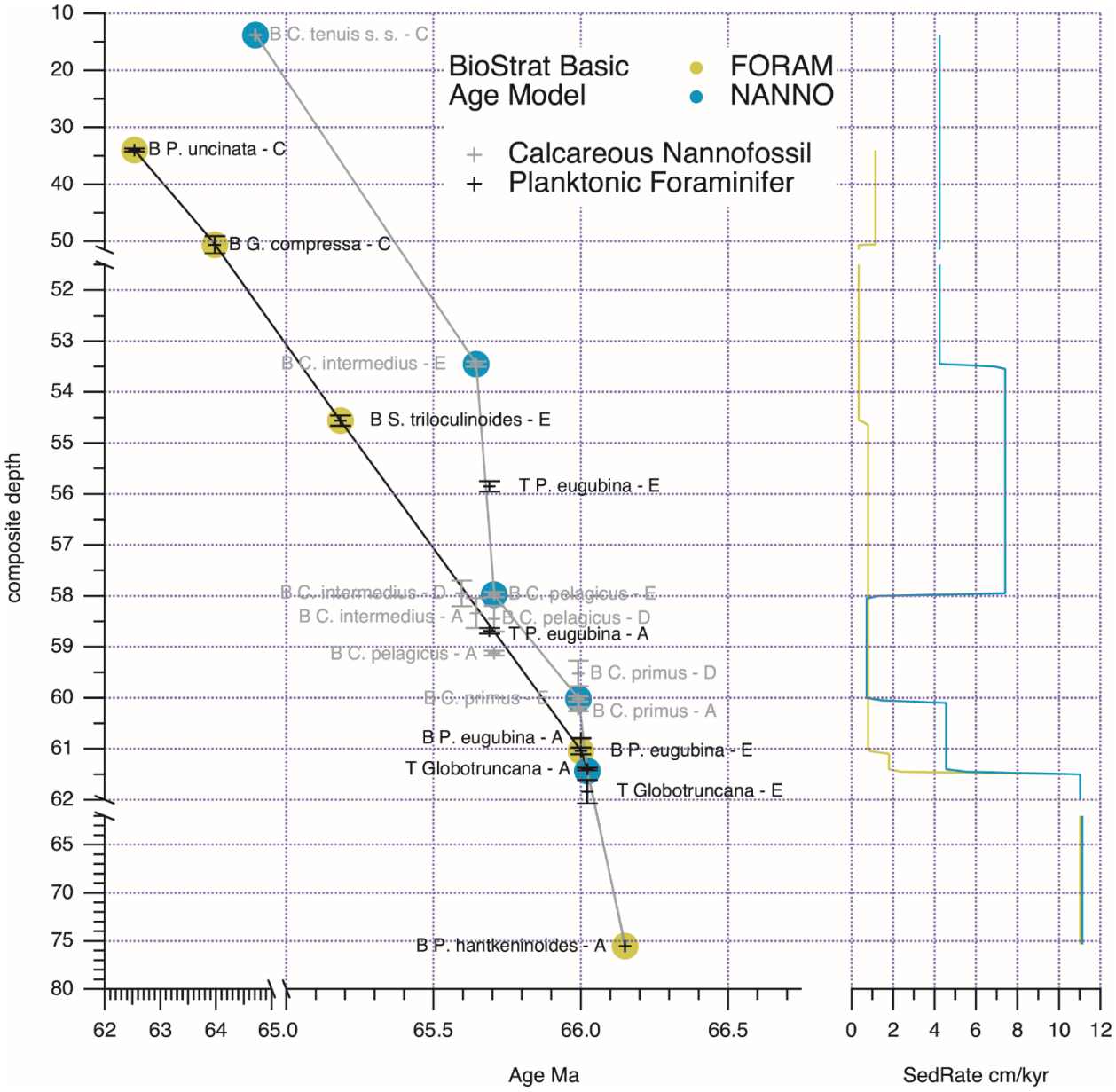

Figure 8. Age-depth model for El Kef is shown.

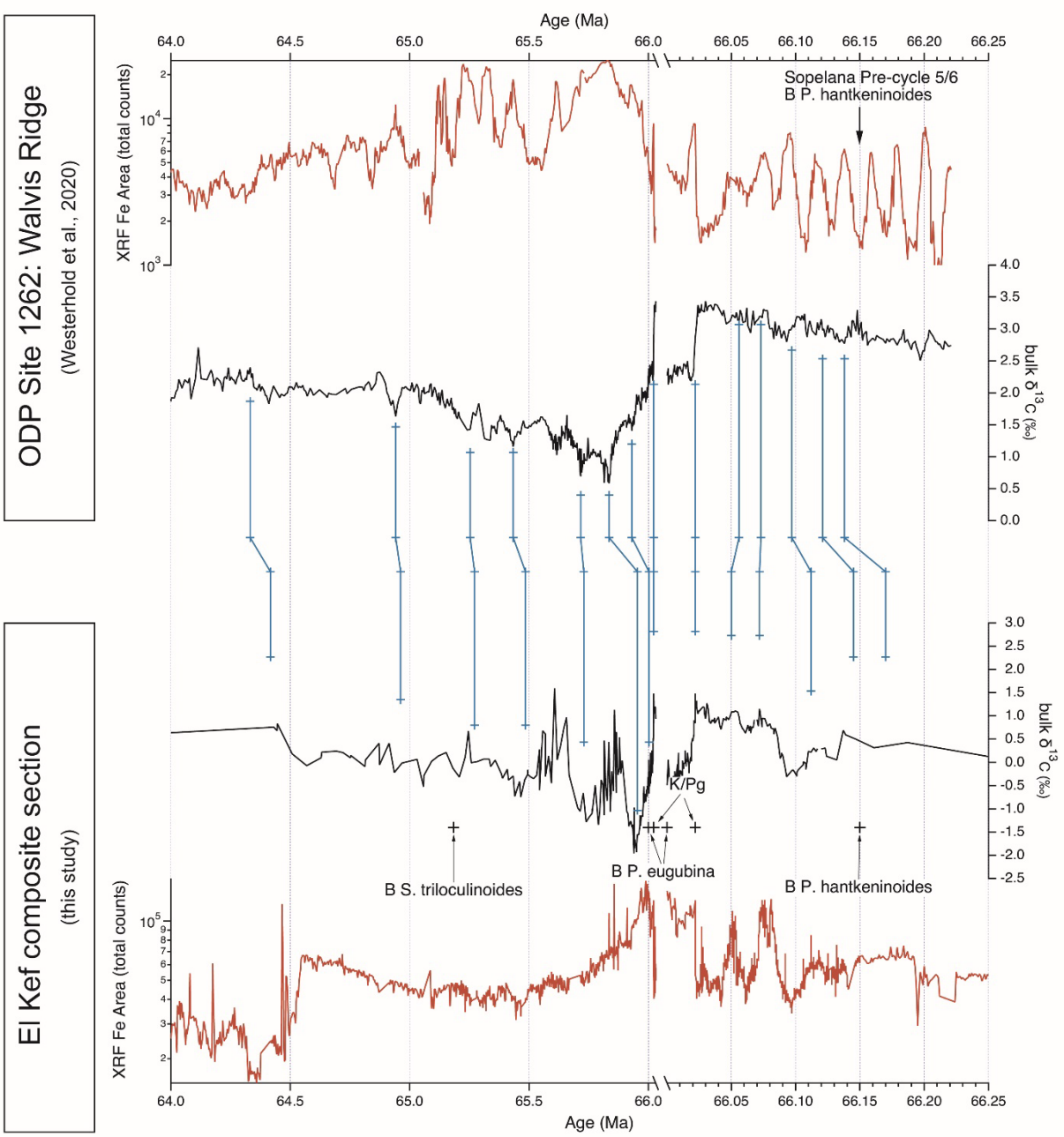

Figure 9. Graph plots correlation of the X-ray fluorescence (XRF) data (red) and bulk carbonate $\delta^{13}C$ records (black) at the El Kef composite section (this study, bottom red and black lines) and at Ocean Drilling Program (ODP) Site 1262 at Walvis Ridge (Westerhold et al., 2020; top red and black lines) using only planktic foraminiferal biostratigraphic datums in the Danian. Tie points are shown as blue lines.

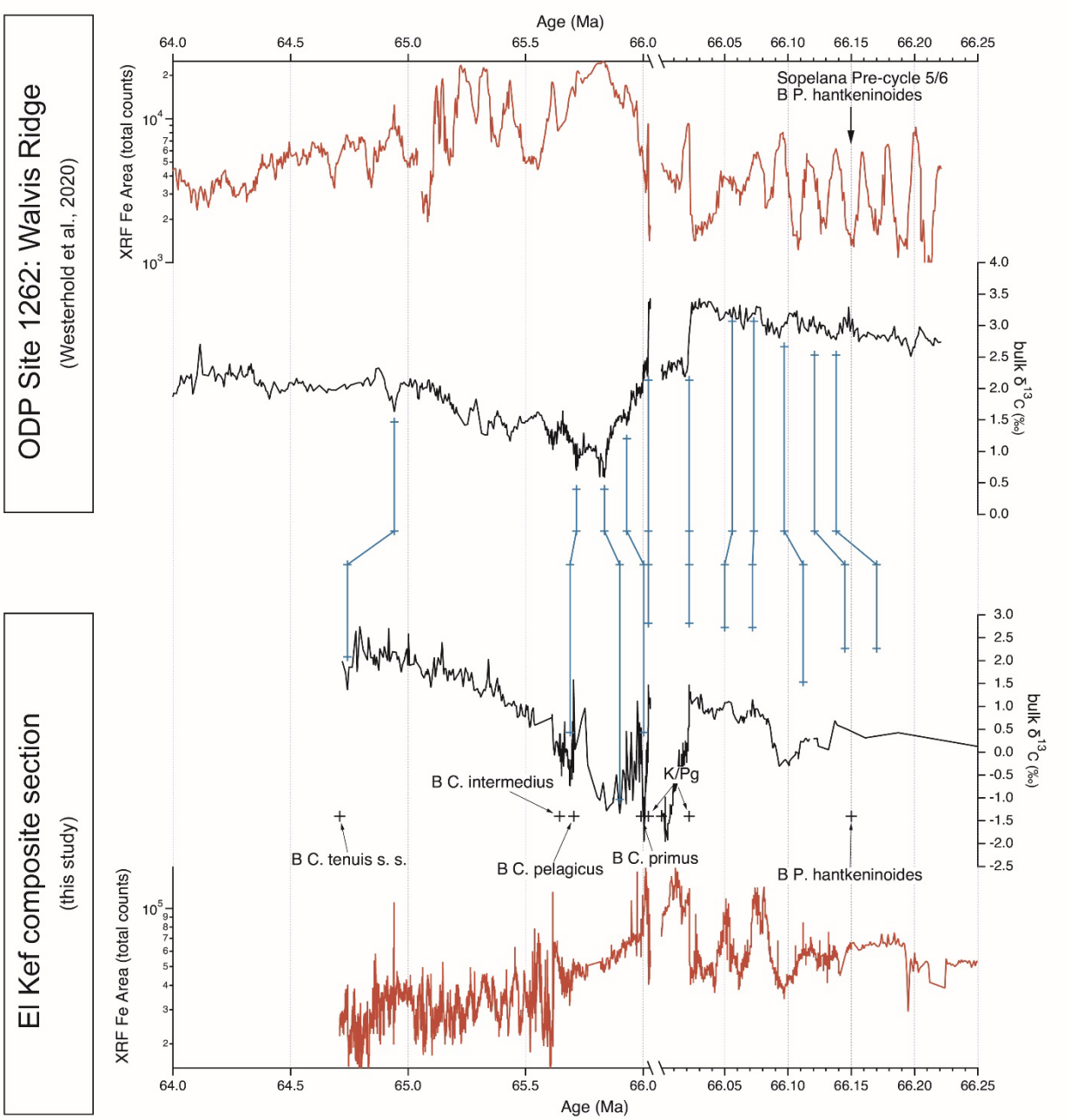

Figure 10. Graph shows correlation of the X-ray fluorescence (XRF) data (red) and bulk carbonate $\delta^{13}C$ records (black) at the El Kef composite section (this study; bottom red and black lines) and at Ocean Drilling Program (ODP) Site 1262 at Walvis Ridge (Westerhold et al., 2020; top red and black lines) using only calcareous nannofossil biostratigraphic datums in the Danian. Tie points are shown as blue lines.

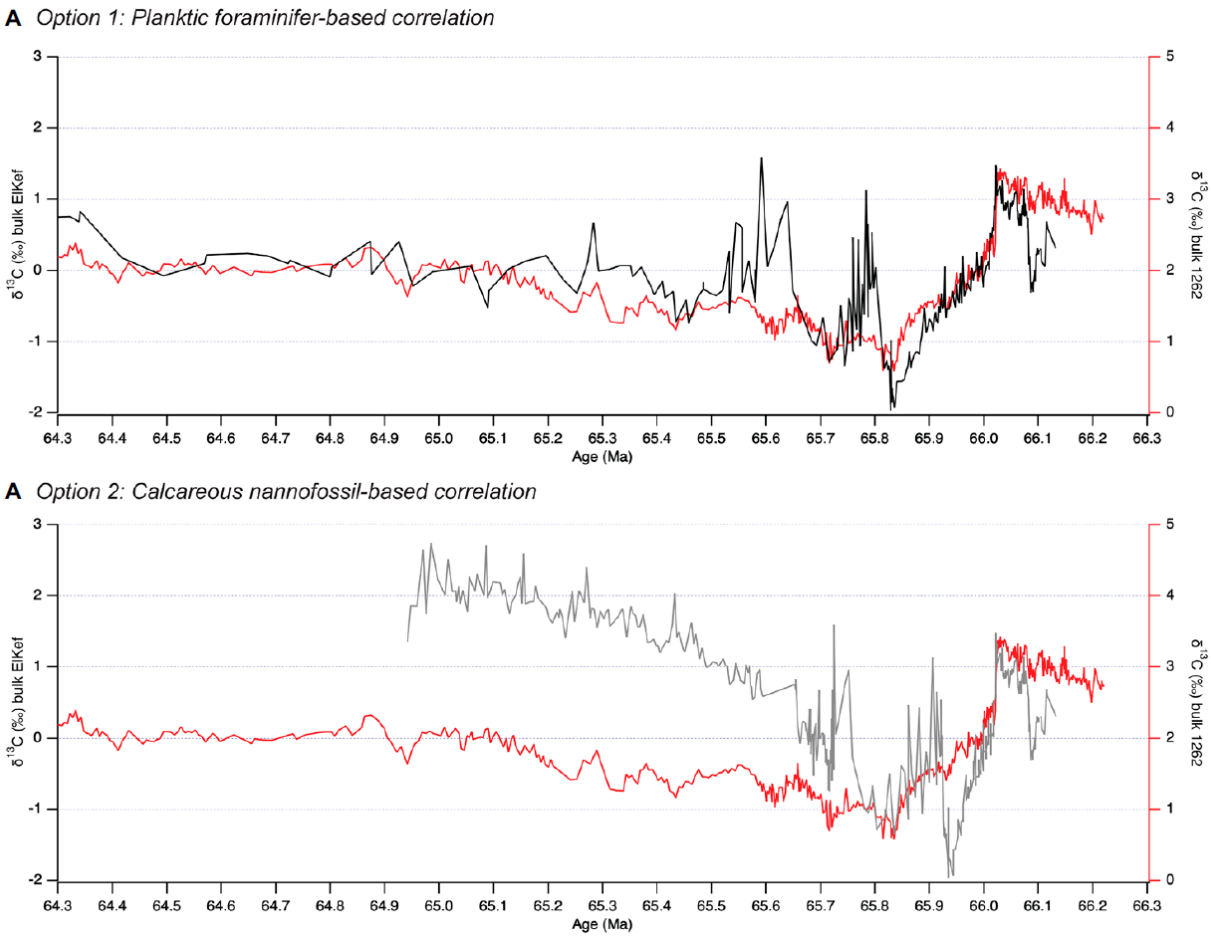

Figure 11. Graphs show correlation of the bulk carbonate $\delta^{13}C$ record from Walvis Ridge (red line) to the composite bulk carbonate $\delta^{13}C$ record from El Kef (black line, top, and gray line, bottom) using (A) only the planktic foraminiferal biostratigraphic datums for the Danian (Option 1) and (B) only the calcareous nannofossil biostratigraphic datums for the Danian (Option 2).

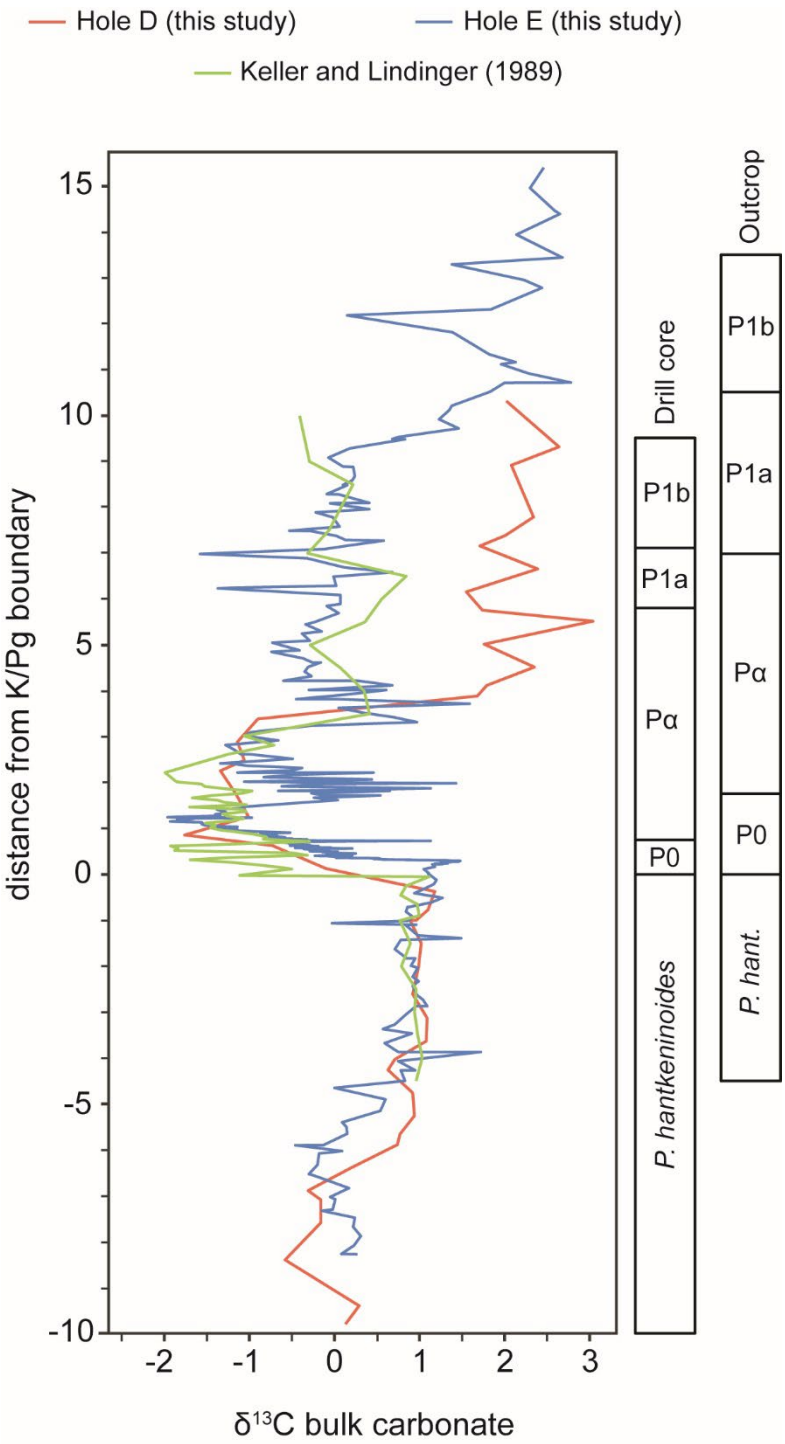

Figure 12. Plot compares bulk carbonate $\delta^{13}C$ records from our El Kef drill cores (Hole D, orange line, and Hole E, blue line) with those from the El Kef outcrop, using data from Keller and Lindinger (1989, green line). We also compare our planktic foraminiferal biostratigraphy from Hole E to the El Kef outcrop (modified from Arenillas et al., 2000).

1612

TABLE 1. PLANKTIC FORAMINIFER AND CALCAREOUS NANNOPLANKTON DATUMS AT EL KEF

Type	Event	Zone	Age estimate (Ma)	Age source	Top			Bottom			Mid	
					ID	Drill depth (m)	Mcd (m)	ID	Drill depth (m)	Mcd depth (m)	mcd depth (m)	± m
PF*	B† *Praemurica uncinata*	P2	62.537	Wade et al. (2011); Gradstein et al. (2012); Westerhold et al. (2020)	El Kef C 14R-1, 73–76 cm	20.45	33.79	El Kef C 14R-1, 123–126 cm	20.95	34.29	34.04	0.25
PF	B *Globanomalina compressa*	P1c	63.978	Wade et al. (2011); Gradstein et al. (2012); Westerhold et al. (2020)	El Kef C 23R-1, 149–150 cm	35.50	49.10	El Kef E 5R-1, 10–12 cm	9.98	52.16	50.63	1.53
CN§	B *Cruciplacolithus tenuis* s.s.#		64.709	Bernaola and Monechi (2007), Westerhold et al. (2020)	El Kef C 2R-1, 100–101 cm	0.60	13.85					
PF	B *Subbotina triloculinoides*	P1b	65.184	Wade et al. (2011); Gradstein et al. (2012); Westerhold et al. (2020)	El Kef E 6R-1, 80–82 cm	12.28	54.46	El Kef E 6R-1, 100–102 cm	12.48	54.66	54.56	0.10
CN	B *Cruciplacolithus intermedius*		65.644	Bernaola and Monechi (2007), Westerhold et al. (2020)	El Kef E 5R-1, 135–136 cm	11.23	53.41	El Kef E 5R-1, 145–146 cm	11.33	53.51	53.46	0.05
CN	B *Cruciplacolithus intermedius*		65.644	Bernaola and Monechi (2007), Westerhold et al. (2020)	El Kef A 13R-1, 118 cm	16.57	58.05	El Kef A 14R-1, 40 cm	17.15	58.63	58.34	0.29
CN	B *Cruciplacolithus intermedius*		65.644	Bernaola and Monechi (2007), Westerhold et al. (2020)	El Kef D 8R-1, 10 cm	14.42	57.70	El Kef D 8R-1, 60 cm	14.92	58.20	57.95	0.25
CN	B *Coccolithus pelagicus*		65.705	Bernaola and Monechi (2007), Westerhold et al. (2020)	El Kef E 8R-1, 100–101 cm	15.75	57.93	El Kef E 8R-1, 110–111 cm	15.85	58.03	57.98	0.05
CN	B *Coccolithus pelagicus*		65.705	Bernaola and Monechi (2007), Westerhold et al. (2020)	El Kef D 8R-1, 60 cm	14.92	58.20	El Kef D 8R-1, 110 cm	15.42	58.70	58.45	0.25
PF	T** *Parvularugoglobigerina eugubina*	P1a	65.690	Wade et al. (2011); Gradstein et al. (2012); Westerhold et al. (2020)	El Kef E 7R-1, 45–47 cm	13.57	55.75	El Kef E 7R-1, 65–67 cm	13.77	55.95	55.85	0.10
PF	T *Parvularugoglobigerina eugubina*	P1a	65.690	Wade et al. (2011); Gradstein et al. (2012); Westerhold et al. (2020)	El Kef A 14R-1, 38–42 cm	17.15	58.63	El Kef A 14R-1, 49–53 cm	17.26	58.74	58.69	0.06
CN	B *Cruciplacolithus primus*		65.991	Bernaola and Monechi (2007), Westerhold et al. (2020)	El Kef E 9R-1, 130 cm	17.64	59.97	El Kef E 9R-1, 140 cm	17.74	60.07	60.02	0.05
CN	B *Cruciplacolithus primus*		65.991	Bernaola and Monechi (2007), Westerhold et al. (2020)	El Kef A 15R-1, 102 cm	18.70	60.18	El Kef A 15R-1, 110 cm	18.78	60.26	60.22	0.04
CN	B *Cruciplacolithus primus*		65.991	Bernaola and Monechi (2007); Westerhold et al. (2020)	El Kef D 9R-1, 10 cm	16.05	59.27	El Kef D 9R-1, 60 cm	16.55	59.77	59.52	0.25
PF	B *Parvularugoglobigerina eugubina*	$P\alpha$	66.000	Wade et al. (2011); Gradstein et al. (2012)	El Kef E 10R-1, 70–72 cm	18.65	60.99	El Kef E 10R-1, 84–86 cm	18.79	61.13	61.06	0.07
PF	B *Parvularugoglobigerina eugubina*	$P\alpha$	66.000	Wade et al. (2011); Gradstein et al. (2012)	El Kef A 16R-1, 40–41 cm	19.39	60.79	El Kef A 16R-1, 41–42 cm	19.40	60.80	60.79	0.01
PF	B *Guembelitria cretacea*	P0	66.022	Wade et al. (2011); Dinares-Turell et al. (2014)	El Kef E 10R-1, 139–140 cm	19.34	61.68	El Kef E 11R-1, 1–2.5 cm	19.59	62.08	61.88	0.20
PF	B *Guembelitria cretacea*	P0	66.022	Wade et al. (2011); Dinares-Turell et al. (2014)	El Kef A 16R-1, 99–100 cm	19.98	61.38	El Kef A 16R-1, 103–106 cm	20.03	61.43	61.40	0.03
CN	*B Cervisiella* acme		66.022		El Kef E 10R-1, 120 cm	19.14	61.48	El Kef E 10R-1, 130 cm	19.24	61.58	61.53	
CN	B *Cervisiella* acme		66.022		El Kef D 10R-1, 60 cm	18.18	61.34	El Kef D 10R-1, 110 cm	18.68	61.84	61.59	
CN	B *Cervisiella* acme		66.022		El Kef A 16R-105	20.03	61.43	El Kef A 16R-110	20.08	61.48	61.46	
Event	K/Pg	K/Pg	66.022	Dinares-Turell et al. (2014)	El Kef D 10R-1, 73 cm	18.31					61.44	
PF	B *Plummerita hantkeninoides*		66.150	Coccioni und Premoli Silva (2015)	El Kef A 25R-1, 75–77 cm	33.88	75.40	El Kef A 25R-1, 103–107 cm	34.17	75.69	75.55	0.15

Note: Mcd—meters composite depth.
*PF—Planktic foraminifer.
†B—Base.
§CN—Calcareous nannoplankton.
#s.s.—sensu stricto.
**T—top.

TABLE 2. BASIC AGE MODEL BASED ON PLANKTIC FORAMINIFERAL BIOSTRATIGRAPHIC DATUMS

Type	Event	Zone	Age estimate (Ma)	Age source	Top			Bottom			Mid	
					ID	Drill depth (m)	Mcd depth (m)	ID	Drill depth (m)	Mcd depth (m)	Mcd depth (m)	±m
PF*	B† *Praemurica uncinata*	P2	62.537	Wade et al. (2011); GPTS Westerhold et al. (2020)	El Kef C 14R-1, 73–76 cm	20.45	33.79	El Kef C 14R-1, 123–126 cm	20.95	34.29	34.04	0.25
PF	B *Globanomalina compressa*	P1c	63.978	Wade et al. (2011); GPTS Westerhold et al. (2020)	El Kef C 23R-1, 149–150 cm	35.50	49.10	El Kef E 5R-1, 10–12 cm	9.98	52.16	50.63	1.53
PF	B *Subbotina triloculinoides*	P1b	65.184	Wade et al. (2011); GPTS Westerhold et al. (2020)	El Kef E 6R-1, 80–82 cm	12.28	54.46	El Kef E 6R-1, 100–102 cm	12.48	54.66	54.56	0.10
PF	T§ *Parvularugoglobigerina eugubina*	P1a	65.690	Wade et al. (2011); GPTS Westerhold et al. (2020)	El Kef E 7R-1, 45–47 cm	13.57	55.75	El Kef E 7R-1, 65–67 cm	13.77	55.95	55.85	0.10
PF	B *Parvularugoglobigerina eugubina*	P_{α}	66.000	Wade et al. (2011); GPTS2012	El Kef E 10R-1, 70–72 cm	18.65	60.99	El Kef E 10R-1, 84–86 cm	18.79	61.13	61.06	0.07
Event	K/Pg	K/Pg	66.022	Dinares-Turell et al. (2014)	El Kef D 10R-1, 73 cm	18.31					61.44	
PF	B *Plummerita hantkeninoides*		66.150	Coccioni and Premoli Silva (2015)	El Kef A 25R-1, 75–77 cm	33.88	75.40	El Kef A 25R-1, 103–107 cm	34.17	75.69	75.55	0.15

Note: Mcd—meters composite depth.
*PF—Planktic foraminifer.
†B—Base.
§T—top.

TABLE 3. ALTERNATIVE BASIC AGE MODEL BASED ON CALCAREOUS NANNOPLANKTON BIOSTRATIGRAPHIC DATUMS

Type	Event	Age estimate (Ma)	Age source	Top			Bottom			Mid	
				ID	Drill depth (m)	Mcd depth (m)	ID	Drill depth (m)	Mcd depth (m)	Mcd depth (m)	± m
CN*	B† *Cruciplacolithus tenuis* s. s.§	64.709	Bernaola and Monechi (2007), Westerhold et al. (2020)	El Kef C 2R-1, 100–101 cm	0.60	13.85					
CN	B *Cruciplacolithus intermedius*	65.644	Bernaola and Monechi (2007), Westerhold et al. (2020)	El Kef E 5R-1, 135–136 cm	11.23	53.41	El Kef E 5R-1, 145–146 cm	11.33	53.51	53.46	0.05
CN	B *Coccolithus pelagicus*	65.705	Bernaola and Monechi (2007), Westerhold et al. (2020)	El Kef E 8R-1, 100–101 cm	15.75	57.93	El Kef E 8R-1, 110–111 cm	15.85	58.03	57.98	0.05
CN	B *Cruciplacolithus primus*	65.991	Bernaola and Monechi (2007), Westerhold et al. (2020)	El Kef E 9R-1, 130 cm	17.64	59.97	El Kef E 9R-1, 140 cm	17.74	60.07	60.02	0.05
Event	K/Pg	66.022	Dinares-Turell et al. (2014)	El Kef D 10R-1, 73 cm	18.31					61.44	
PF#	B *Plummerita hantkeninoides*	66.150	Coccioni und Premoli Silva (2015)	El Kef A 25R-1, 75–77 cm	33.88	75.40	El Kef A 25R-1, 103–107 cm	34.17	75.69	75.55	0.15

Note: Mcd—meters composite depth.
*CN—Calcareous nannoplankton.
†B—Base.
§s.s.—sensu stricto.
#PF—Planktic foraminifer.